Surface Enhanced Fluorescence: A Classic Electromagnetic Approach

by

Zhe Zhang

A Dissertation Presented in Partial Fulfillment
of the Requirements for the Degree
Doctor of Philosophy

Approved June 2013 by the
Graduate Supervisory Committee:

Rodolfo Diaz, Co-Chair
Derrick Lim, Co-Chair
George Pan
Hongyu Yu

ARIZONA STATE UNIVERSITY

August 2013

ABSTRACT

The fluorescence enhancement by a single Noble metal sphere is separated into excitation/absorption enhancement and the emission quantum yield enhancement. Incorporating the classical model of molecular spontaneous emission into the excitation/absorption transition, the excitation enhancement is calculated rigorously by electrodynamics in the frequency domain. The final formula for the excitation enhancement contains two parts: the primary field enhancement calculated from the Mie theory, and a derating factor due to the backscattering field from the molecule. When compared against a simplified model that only involves the primary Mie theory field calculation, this more rigorous model indicates that the excitation enhancement near the surface of the sphere is quenched severely due to the back-scattering field from the molecule. The degree of quenching depends in part on the bandwidth of the illumination because the presence of the sphere induces a red-shift in the absorption frequency of the molecule and at the same time broadens its spectrum. Monochromatic narrow band illumination at the molecule's original (unperturbed) resonant frequency yields large quenching. For the more realistic broadband illumination scenario, we calculate the final enhancement by integrating over the excitation/absorption spectrum. The numerical results indicate that the resonant illumination scenario overestimates the quenching and therefore would underestimate the total excitation enhancement if the illumination has a broader bandwidth than the molecule. Combining the excitation model with the exact Electrodynamical theory for emission, the complete realistic model demonstrates that there is a potential for significant fluorescence enhancement only for the case of a low

quantum yield molecule close to the surface of the sphere. General expressions of the fluorescence enhancement for arbitrarily-shaped metal antennas are derived. The finite difference time domain method is utilized for analyzing these complicated antenna structures. We calculate the total excitation enhancement for the two-sphere dimer. Although the enhancement is greater in this case than for the single sphere, because of the derating effects the total enhancement can never reach the local field enhancement. In general, placing molecules very close to a plasmonic antenna surface yields poor enhancement because the local field is strongly affected by the molecular self-interaction with the metal antenna.

To my lovely wife Jin Zou

ACKNOWLEDGMENTS

My deepest gratitude is to my advisor, Dr. Rudy Diaz. I have been amazingly fortunate to have an advisor who gave me the freedom to explore on my own, and at the same time the guidance to recover when my steps faltered. Dr. Diaz mentored me how to think as an engineer and how to justify and realized our ideas. His patience and support helped me overcome many crisis situations and finish this dissertation. My co-advisor, Dr. Derrick Lim, has been always there to listen and give advice. I am deeply grateful to him for the long discussions that helped me figure out the technical details of my work. I am grateful to have Dr. Hongyu Yu and Dr. George Pan as my committee member, who provide insightful comments and constructive criticisms at different stages of my research.

I am also indebted to the members of the Material-Wave Interactions Laboratory with whom I have interacted during the start of my graduate studies. Particularly, I would like to acknowledge Mr. Richard Lebaron, Dr. Sergio Clavijo, Dr. Tom Sebastian, Mr. Paul Hale, Mr. Evan Richards and Ms. Mahkamehossadat Mostafavi for the many valuable discussions that helped me understand my research area better.

TABLE OF CONTENTS

Page

LIST OF TABLES

LIST OF FIGURES

Chapter 1

INTRODUCTION

In the biological and biomedical applications, noble metal nano-particles have been widely used for detection for their unique electromagnetic properties in the Optical frequency range [1, 2, 3, 4, 5, 6, 7, 8, 9, 10]. One of the emerging important applications is enhancing dye molecule emission or quenching for heat or signal generation, by linking the molecule and the particle (viewed as a Plasmon Resonance sphere) based on DNA assembly [1]. The problem is that with the Plasmon resonant particle, specifically spherical, it is hard to tell whether the fluorescence will be enhanced or quenched based on recent experimental results [10, 11, 12]. Reconciliation of the conflicting results is not necessarily straightforward because the interactions among the incident waves, emission waves, Dye molecule and the nano-particles are complicated quantum-electrodynamics problems.

The molecules, which were treated as a three level system in Quantum mechanics, emit the light at a frequency different from the absorption frequency: A fluorescence molecule absorbs energy at a short wavelength λ_{21}, and then degenerates from its initial excited state to a lower energy excited state, and then emits energy at a long wavelength λ_{31}. In the presence of a Plasmon resonant sphere, both the λ_{21} absorption and λ_{31} emission processes are influenced. Das and Metiu [13, 14] utilized the Quantum Mechanics theory to take the particle effects into account. However, their theory is only usable for very small nano-particles and it assumes the absorption dipole moment is so

small that the perturbation on the local field is negligible when compared to the Mie scattering field by the sphere.

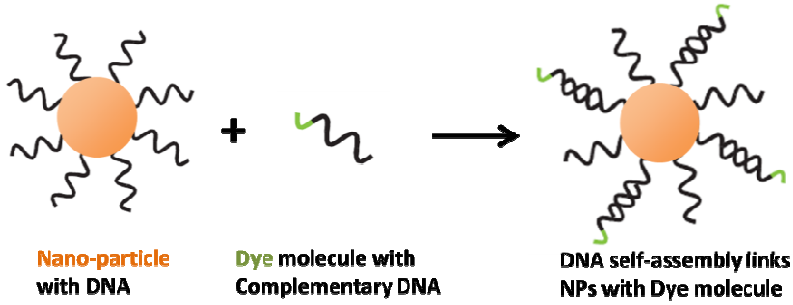

Fig. 1-1 DNA Assembly for fluorescence enhancement or quenching

These surfaced enhanced fluorescence phenomena were actually studied theoretically several decades ago when people investigated the huge fluorescence enhancement and quenching rough metal surfaces. Early work by Purcell [15] indicated that the environment, such as sphere, surface or cavity modifies the radiative property of quantum emitters like atoms and fluorescent molecules. Not only influencing the radiative rate, Plasmonic spheres provide extra non-radiative channels through their dielectric losses. The large induced dipole moment at the resonance of the sphere implies large current flow inside the sphere, which offers possible enhancement through radiation, and possible quenching though dielectric loss [16, 17, 18, 19, 20]. The enhancement or quenching comes from the trade-off between these two competitive elements [6]. Most electromagnetic and quantum mechanical models of the phenomenon [17, 20, 21, 22] claim that fluorescent modifications come from two separate parts: local field excitation rate γ_{exc} modification and the emission quantum yield γ_r/γ modification. This separate

treatment is legitimate, since the absorption and emission operate at different frequency that eliminates the coherence.

For weak excitation where spontaneous emission dominates, the total fluorescent rate γ_{em} can be expressed as [10, 6],

$$\gamma_{em} = \gamma_{exc}[\gamma_r/\gamma] \tag{1-1}$$

where γ_{exc} is the excitation rate, γ_r is the radiative rate, and γ is the total decay rate for emission. The quantum yield $QY = \gamma_r/\gamma$ is defined as the ratio between the radiative rate and the total decay rate of the molecule with the change of environments. According to the Fermi Golden rule, the excitation rate is proportional to the square of the perturbing Hamiltonian $|\boldsymbol{p} \cdot \boldsymbol{E}(\boldsymbol{r_m}, \omega)|^2$, where $\boldsymbol{E}(\boldsymbol{r_m}, \omega)$ is the local electric field and $\boldsymbol{p}$ is absorption transition dipole moment. Assuming that the absorption transition dipole moment is a constant, the total enhancement modification factor K_{tot} can be re-written as the combination of absorption modification K_{exc} by local field and quantum yield adjustment K_{em} in the emission process,

$$K_{tot} = \frac{\gamma_{em}}{\gamma_{em0}} = \frac{\gamma_{exc} QY}{\gamma_{exc0} QY_0} = \frac{\left|\boldsymbol{e_p} \cdot \boldsymbol{E}(\boldsymbol{r_m}, \omega)\right|^2}{\left|\boldsymbol{e_p} \cdot \boldsymbol{E_0}(\boldsymbol{r_m}, \omega)\right|^2} \cdot \frac{QY}{QY_0} = K_{exc} \cdot K_{em} \tag{1-2}$$

where the subscript 0 means the corresponding quantity in the free space or solution.

The modification of quantum yield K_{em} and its contribution to fluorescent enhancement/quenching effects has been well understood for over three decades [17, 18]. In 1980s, several analytical theories based on classical electromagnetics for single molecule emission near a single sphere/plane. An electrostatic theory by Gersten and Nitzan [17] to calculate the radiative rate and non-radiative rate was widely used for quenching and enhancing by spheres or spheroid. Ruppin [18] and Chew [19] published

the theories using the exact electrodynamics. However, the upon Ruppin's theory and re-calculated the total decay rate by using the electric field susceptibility. All these classical theories contain infinite sums over multipole terms, and can only be applied to the single molecule interaction with a single sphere. In 2005, Carminati and Greffet [21] proposed a simple method to model a metallic nano-particle as single dipole moment at the center of the sphere. The radiative rates and total decay rates are then derived using a simple dipole-dipole coupling approach. However, this model has a limitation : when the distance from the emitter to the sphere gets closer than the radius, the centered dipole model for spheres is invalid.

Generally, then, three kinds of methods have been used to analyze this problem: the Electrodynamical method, the quasi-static method, and the dipole-dipole interaction method. Obviously, the Electrodynamical method would provide the most accurate predictions, since it is the strictest one. Nevertheless it is instructive to compare with the other two methods to find out the limitations introduced by the approximations.

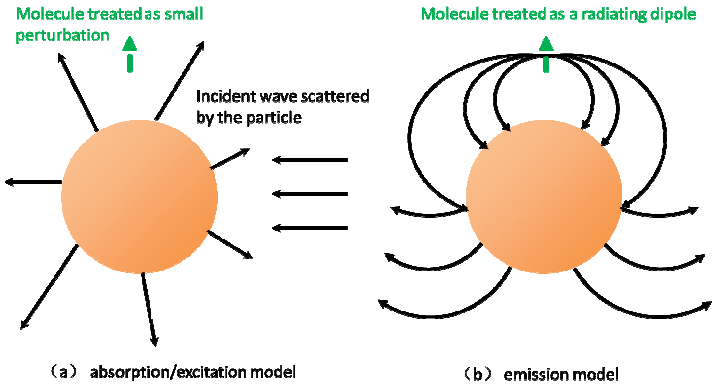

Fig. 1-2 the general electromagnetic modeling for the absorption/excitation and emission

Interestingly, another important part of the phenomenon, the absorption modification has been treated in an extremely simple way: while the molecule was modeled as a radiating dipole in the emission modifications, it was treated as a negligible perturbation on the local field during absorption. Thus, the absorption enhancement was simplified to be the ratio of the local light intensity in the presence of the sphere to the local light intensity without the sphere. Under this assumption the local electric field can be strictly calculated by the Mie theory for simple spherical structures.

However, this simplification leads to a contradiction. Since the fluorescent molecule is an electrically small resonant dipole, consider the case when said dipole has strong scattering at the absorption frequency. From the textbooks on antenna theory, we have the extinction cross section of such a matched dipole as $\lambda^2/4\pi$. Suppose we put such a fluorescent molecule near a Silver nano-sphere (15nm radius) at its resonant frequency 360 nm wavelength. The calculation shows that, if we use the 1V/m plane wave incident on the sphere, the sphere would generate a local field 10 times stronger. From the viewpoint of previous articles in the literature, the molecule should get an absorption enhancement of 100 times (the square of the field enhancement). In the other words, the extinction cross-section becomes $100*\lambda^2/4\pi$. However, when you treat the molecule-sphere as one antenna system, entirely enclosed within a region 20nm on the side, the system is still electrically small and by definition its maximum extinction cross section cannot exceed $3*\lambda^2/2\pi$ [23]. Therefore the simplification that the total local field is only due to the incident wave interacting with the sphere artificially overestimates the extinction cross section of the molecule, which also overestimates the molecule absorption ability. Such a contradiction could be resolved by Classic Electrodynamics:

The dipole molecule generates its dipole field, and this field is scattered back into the dipole again by the sphere; the strong oscillation and short distance between the molecule and the particle makes the re-scattering so strong that is not negligible when compared with the plane wave plus its scattering field (we will call that the Mie field instead). The whole process can make the local field very different from the Mie field.

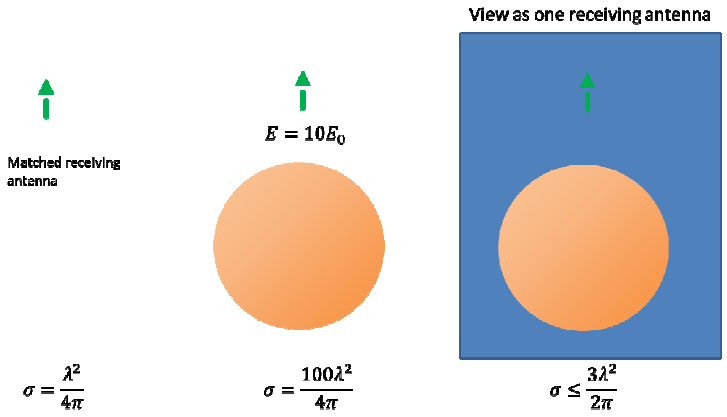

Fig. 1-3 the contradiction between simplified modeling neglecting the dipole field in absorption

This contradiction requires us to re-derive the equations for fluorescence enhancement from Quantum Mechanical viewpoint into the electromagnetics. The dipole field influence has to be considered and implemented into the absorption equations.

The dissertation is organized as follows: In Chapter 2, a literature review is performed to highlight the experimental disagreement on fluorescence quenching and enhancement. Several different theoretical explanations are discussed. In Chapter 3, we demonstrate the validity for separating the absorption and emission calculation, and establish the correct electromagnetic model of the fluorescence from the quantum mechanical viewpoint. In Chapter 4, the emission models are discussed. We compare the

Gerstern-Nitzan model, exact electrodynamical model and Carminati's model. Based on the image theory, we develop a simplified model for the emission quantum yield enhancement. The back-scattered field from the unit dipole is utilized in the total decay rate calculation. In Chapter 5, we derive the local field on the molecule with the consideration of the molecular spontaneous emission field. The results show the possibility of quenching of the excitation due to the self-field term. The absorption frequency is shifted and the bandwidth is broadened due to the sphere. Hence, for broadband illumination, integration over the spectrum is required for accuracy in the excitation enhancement. The final results show that the excitation enhancement is almost always derated by the backscattered self-field. However, the frequency domain results that only consider the resonant frequency illumination would overestimate this effect. In Chapter 6, we develop the general method to estimate the total fluorescence enhancement. The total enhancement is separated into the primary field enhancement, derating factor, and the emission quantum yield enhancement by the nano-antennas. Once we compare the numerical results for the spherical antenna to exact electrodynamical results that we derived and summarized in Chapter 4-5, we conclude that the finite difference time domain method (FDTD) provides precise far field and near field computations. We apply the method for the spherical dimer antenna, the excitation enhancement is strongly dependent on the derating factor. In Chapter 7, we summarize the theoretical work for the fluorescence enhancement from the electromagnetic theory viewpoint.

Chapter 2

EHANCEMENT AND QUENCHING BY METALLIC STRUCTURES

2.1 Introduction

The interaction between photosensitive molecules and the electromagnetic field in the vicinity of metal nanostructures is at the heart of a multitude of applications ranging from the measurement of microscopic distances during molecular reactions [24] to the development of more efficient solar cells [25, 26]. The purpose of the metal nanostructures is to change the "response" of the photosensitive molecules. Paradoxically, when the change is measured using fluorescence, the results in the literature are almost equally likely to show quenching of the radiation as to show enhancement of the same.

Although the discrepancy in results must be attributed to differences in the details of the experiments, there does not appear to be a systematic accounting in the literature of the relationship between those differences and the final result (quenching or enhancement). Since it is straightforward to enumerate the experimental parameters that could possibly contribute to this difference, the lack of a categorical verdict reveals a more fundamental problem. This problem appears to be an uncertainty about the "Physics" involved in the interaction.

For example, in the mid 2000's several papers sought to explain quenching results in terms of a new postulated phenomenon called Nanometal Surface Energy Transfer (NSET) [27]. The quenching data was fitted to an inverse power law and shown to differ from the 6th power law of ordinary Förster's Resonant Energy Transfer (FRET) and

closer to a 4th power law. From the resemblance of this power law to the interaction between a dipole and a conducting plane it was then speculated that “planes” of dipoles in the metal particle were responsible for this unusual behavior. However, in light of the boundary conditions obeyed by Maxwell’s equations at a material boundary, and the fact that classical electrodynamics solutions obey linear superposition, such an explanation is a logical impossibility.

Even in the case when full physics computational electrodynamics methods are used to support enhancement data we find similar uncertainties. For instance, Lakowicz and his collaborators [28] applied the Finite Difference Time Domain (FDTD) method to calculate the electric field in the neighborhood of a metal nanoparticle. After obtaining their results, the authors are careful to state that their experimentally observed enhancement of fluorescence is *consistent* with the enhanced Electric field intensity calculated; but they advance no precise quantitative predictions to be compared to the data.

These same authors have repeatedly emphasized the importance of the nanoparticle size in supplying enhancement by positing the rule that whenever the particle’s scattering cross section exceeds its absorption cross section, enhancement is to be expected. Yet this is a rule derived from the far field plane-wave scattering properties of a nanoparticle and it is not explained why it should be expected to apply to the case of a molecule whose near field interacts with the nanoparticle quite differently from a plane wave. They also have proposed that a minimum distance of the order of 11 nm is optimal for enhancement effects, yet again there is no *precise* electrodynamical rationale given for this number.

In 2006, Novotny [6, 7] analyzed the fluorescence enhancement and quenching effects due to distance variation from one single silver sphere using Classical Electromagnetics. Even though he used the quasi-static approximations, the process of the treatment was convincing: The excitation enhancement and the emission enhancement were calculated separately and combined for total fluorescence enhancement. However, we have to notice that the excitation enhancement calculation not only assumed the dipolar scattering by sphere in near field, but also *ignored the molecule's existence*. In the other word, the self-scattering field from the *molecule* at the excitation frequency was never considered in the picture.

It is one purpose of this dissertation to shed light on the origin of the apparent contradictions and uncertainties seen in the literature. The solution of the dilemma has been known since the work of Das and Metiu in 1985 [13]. In fact, our work can be considered a companion to Das' 2002 paper [14] where he reiterated his results considering the molecular re-radiation in terms of the molecule image field in the quantum mechanical model. Even though the original papers [13, 14] proposed the consideration of the re-radiation field effect for absorption/excitation, it was limited to the electric *small sphere*. Similar considerations on the *re-radiation effects* were applied to the resonant Raman enhancement [29, 30]. In Sun's paper [30], the *re-radiation effects* are explicitly applied to modeling resonant Raman enhancement, but not considered for the case of excitation for fluorescence enhancement. Our approach expands Das and Sun's considerations of *re-radiation* by solving the problem from the standpoint of modern electromagnetic engineering, using both antenna theory and full physics

computational electrodynamics methods to consider arbitrarily sized and arbitrarily shaped particles.

2.2 The case for quenching

As noted above the authors of [27] consistently measure quenching of fluorescence. Since the nanoparticles they used were extremely small (diameter d=1.4nm), their far field extinction cross section is completely dominated by absorption. Therefore if the rule that enhancement depends on the scattering cross section exceeding the absorption cross section is true, this result would be expected. However the experiments of Ray et al [24] appear to show pervasive quenching even with particles as large as 70nm in diameter, and the behavior to be unexplained by either FRET or NSET.

Quenching of QDs closer than 4nm from a metal surface is predicted by Larkin et al [31] on the grounds of a non-classical local random phase approximation. But at these distances other non-classical effects have been postulated that may have the same effect such as non-local behavior in the dielectric function of the metal [32]. The problem with these very small distances from the surface is that once we are in the 2-4 nm range other physico-chemical phenomena come into play that can lead to non-electrodynamic quenching, such as electron-hopping or physical alteration of the molecule's energy levels due to extreme proximity to the metal surface. These "contact" phenomena may be dramatically different for an organic molecule and a quantum dot. Specifically if electron hopping from the molecule to the metal nanoparticle occurs either along the tether (that separates it from the nanoparticle) or through the surrounding solution we would have a

mechanism for quenching in molecules. The fact that quantum dots are insulating dielectrics may mean they have a built in barrier against this quenching channel.

Therefore when determining the enhancement or quenching properties of a given molecule-nanostructure combination using conventional Physics (electrodynamics or quantum mechanics), in which the material structure is assumed to have a well-defined dielectric function, we should assume distances greater than 4 nm. Any quenching that occurs beyond 4 nm must be explainable by conventional theory.

Experimental results often include data in this applicable range. For instance, Schneider and Decher [4] proved that when fluorescin and lissamine photoluminescent dyes are placed 1.5 nm to 8nm from 13nm gold nanospheres, their photoluminescence is quenched; the closer they are the more severe the quenching. Similarly, Dulkeith [1, 2] reported quenching of Cy5 chromophore fluorescence by 12 nm gold nanoparticles from 2 to 16 nm separation. But the authors stated that it is known that at 10 nm over structured metal surfaces enhancement occurs.

2.3 The case for enhancement

Two electrodynamic phenomena are expected to contribute to enhancement. The first is the concentration of an incident plane wave electric field into near field “hot spots” by the plasmon resonance of the noble metal structure. This is well known and documented in the Surface Enhanced Raman Scattering literature. The second is the increase in radiation resistance [33] available for emission due to the coupling of a large antenna (the particle) to the smaller antenna (the molecule). This is usually expressed as a

Radiative Rate increase [34, 35]. Experimental evidence for enhancement measured as fluorescence enhancement also abounds in the literature.

In 2001 Lakowicz [8] reported an 80-fold increase of fluorescence from DNA (extremely poor fluorophore) near silver islands. Kulakovich et al [36] obtained a maximum luminosity enhancement for quantum dots of the order of five times at 11 nm separation between the quantum dots and a gold colloid surface. The colloid surface was formed using particles 12nm to 15nm in diameter. Louis et al, [37] show that 15 nm gold particles coated with 3 nm Rare Earth (RE) particles exhibit fluorescence intensity enhancement of the RE by 42 times. In their experiment the RE oxide particles were in direct contact with the gold nanoparticle. When they used larger RE particles, thus increasing the mean distance of the radiating center from the surface, the enhancement went down to only 7 times.

In a slightly different configuration Zhang et al [5] worked with silica beads with average diameters in the range of 40-600 nm, with Ru(bpy)3 2+ complexes incorporated into the beads that were then over-coated with a continuous but porous silver shell 5-50 nm thick. Enhancement as high as 16 times was obtained for small core beads with shells of the order of 40 nm thick. Kuhn et al [38] used an apertureless NOSM configuration to demonstrate up to 19 times enhancement in radiated intensity by a terrylene molecule embedded in a 30 nm paraterphenyl 20 (pT) film and a simultaneous drop in decay time from 20ns (the typical value for such molecules at the air-pT interface) to 1 ns (below the 4ns in-the-bulk value) as a result of bringing a 10 nm gold nanosphere within 1nm of the film.

In a different phenomenon, Chowdhury et al [39] show 20 times enhancement of chemi-luminescence when a 1 micron thick layer of solution is sandwiched between glass plates covered with non-continuous silver deposits with islands approximately 200 nm in diameter, 40 nm high. Estimating that the enhancement is only effective within 10nm of the surface the authors postulate that the actual enhancement was probably closer to 100 to 1000 times per molecule. In the chemi-luminescence case the absorption enhancement side of the fluorescence experiment is obviated.

2.4 Seeking an explanation

The variety of results reported above must be related to the differences in the experimental conditions. Using a purely electrodynamical point of view we can highlight these differences and their expected contribution as follows: First, all the radiators used were not the same. In Table 2-1, given specific quantum yield, it is clear that different experiments used radiators of different intrinsic efficiency [40, 41].

QY	≈ 0.92	≈ 0.94	0.15	0.25
Radiator	Fluorescein	Rhodamine 6G	Tetraphenyl porphyrin	Cy5.5

Table 2-1 Variation in Quantum Yield of the radiators

Second, in electromagnetic theory it is well known that the efficacy with which a material structure couples electromagnetic energy into free space depends on the modes it can support. Certain surfaces can decrease a radiator's output by redirecting power into trapped modes (a dielectric plane) or into material loss (a poor conductor) whereas other structures (periodic gratings or plasmon resonant particles) can enhance radiation by coupling the evanescent waves of the radiator's near field into propagating waves. To the

degree that the two kinds of phenomena can exist on the same structure, to this degree the results can be mixed (e.g. a lossy plasmon-resonant nanoparticle). The following are the kinds of structures used in some of these experiments with their expected effect on the radiator's output to the far field.

Effect	Decrease	Moderate Increase	Increase	Larger Increase
Structure	Dielectric films or smooth metal films with no out-coupling prism.	Noble metal nanoparticles at the Plasmon resonance frequency	Noble metal particles large enough to sustain higher order modes on their surface	Rough or periodic large Noble metal surfaces

Table 2-2 Variation of free space coupling in the structures

Third, the ohmic loss mechanism of a nanostructure depends not only on the intrinsic composition (normally used Ag is less lossy than Au) but also on the morphology of its surface, particularly in relation to the conduction electrons' mean free path. If material boundaries are closer than the mean free path (thin films, small particles) [42], the excess collisions increase the loss experienced by the electromagnetic field and reduce the field enhancement. However, the way the material boundaries shape the radiator's near field also affects the induced currents and loss in the material. Thus in the presence of a colloidal quasi-crystal we might see two different phenomena. A radiator very close to the crystal's surface may interact strongly with only one sphere and yield the results expected for a small isolated sphere while increasing the distance from the crystal surface will bring in a collective interaction that will tend to make the material "look" like a large planar boundary. Therefore, we expect the radiation enhancement of

realistically lossy Noble metal structures in the different experimental approaches to be different.

Enhancement	Lowest	Low	Mediocre	Moderate	Higher	Highest
Structure	Au 10nm spheres	Au 15nm spheres in a colloid in near field	Au colloid farther away (responds as a surface)	Au 100nm spheres	Ag 40nm shells	Ag 200nm islands

Table 2-3 Enhancement taking into account ohmic loss

Finally, as pointed out in [34] the radiation rate of a radiator is measured in antenna theory as the radiation resistance of the antenna. For electrically small objects this quantity is proportional to $(l/\lambda)^2$ and measured in ohms, where l is the largest dimension of the radiator. It follows that the power radiated to the far field is proportional to this quantity and so is the radiation efficiency. Therefore in terms of output power to the far field we expect:

Efficiency	Lowest	Low	Moderate	Moderate	High
Radiator	RE 3nm spheres	Au 10nm – 15nm spheres	Au 100nm spheres	Ag shells with 200nm core	Ag rough surface with 200nm islands

Table 2-4 Variation of radiation efficiency of Plasmon Antenna due to size

The large variation in results exemplified above has been noted and addressed by other authors. Bene et al [3] explain their results in terms of the Gertsen-Nitzan (GN) model [17], which utilized purely classical electrostatic theory. Therefore they expect quenching to occur at close distances and enhancement to occur at intermediate distances from the surface of the particle. Casting their explanation in the language of FRET, they

speak of the spectra of a nanoparticle in the same terms they speak of the spectra of fluorophores. This leads to the claim that enhancement should occur for their dyes at *some* optimal distance from the surface of the gold nanoparticles because the "local field enhancement" spectrum of the particle overlaps both the absorption and emission spectrum of the dye while the "absorption spectrum" of the particle has little overlap with the emission spectrum of the dye.

In stating the expectation this way these authors are using the far field scattering and absorption cross sections of the particle as guidelines for the way it will couple to a dye molecule in the near field. This viewpoint is partially related to the considerations of Table II and Table IV above but it confounds near field phenomena with far field phenomena. They correctly point out that enhancement can occur provided the unperturbed QY of the molecule is low enough.

Similarly, Anger et al [6] state that the contradicting reports of enhancement and quenching arise from the different distance dependence of radiative rate increase and nonradiative transition rate increase due to the NP. This is a combination of the considerations in Tables III and IV above. The nonradiative transition rate is equivalent to the ohmic loss suffered by the near field of the radiator and the radiative rate increase is the enhancement in radiation efficiency. However these authors do not appear to consider the initial QY of the molecule to be a factor (the parameter of) and so they assume a high QY molecule.

Yet as mentioned by Bene et al [3] it matters. Radiation efficiency is always a competition between the radiation resistance of the antenna and all other loss mechanism resistances. A low QY (short lifetime in Table I) is equivalent to a large loss resistance

within the radiator and it must be taken into account just like the loss within the nanoparticle is taken into account.

Other authors have sought the root of the problem in oversimplifications of the electrodynamic model, for instance in the omission of higher order terms in the Mie expansion that modify the local field enhancement [43]. But such corrections are only relevant when the Noble metal particle is either large enough to support those modes or when the loss of the particle is assumed to be unrealistically low. The omission of the excitation of "dark modes" by a proximate point dipole source has also been offered as an explanation. These dark modes are the higher order multipoles of the nanosphere's response that, not being resonant, are more lossy than radiating. Although a plane wave excites only primarily the electric dipole mode on a plasmon resonant sub-wavelength sphere, the highly asymmetric near field of a proximate point source can and will excite many more modes. Therefore it is clear that a single, centered image dipole approximation to the response of the sphere to a nearby radiator is not sufficient [21, 44].

If oversimplification of the electrodynamical treatment is the culprit then the widespread use of the Gertsen Nitzan (GN) model [17] would be suspect because this classic model assumed quasi-electrostatics is sufficient to explain the response of the sphere and omits the phase retardation effects intrinsic to wave phenomena. This may explain why some authors take the GN model as a qualitative guide rather than a quantitative tool. Dulkeith et al [1] find a two order of magnitude discrepancy between the calculated rate of resonant energy transfer and their experimentally determined nonradiative rates, even though the shape of the curves (as a function of nanoparticle size) are similar. The discrepancy is blamed on (a) the GN model missing non-local

effects, (b) the point dipole model of the molecule being inadequate, (c) the possibility that not all the molecules were exactly parallel to the particle surface or (d) that a spectral overlap integral was not used for the calculation.

Colas de Francs et al [11] did full Mie theory of the emission-only problem. It is stated that a requirement for the dipolar model of the molecule to be applicable is the weak coupling regime. Their reference is the work of Klimov et al [45] where the variation of the resonance frequency and line-width of an oscillator in the presence of a dielectric sphere were given in the weak coupling limit.

As will be shown in Sections 3 and 4 the inadequacy of the point dipole model has less to do with size and more to do with ignoring the other physical antenna properties of any radiator. The results of Klimov correspond, without qualification of weak or tight coupling, to the modification of the circuit parameters of the antenna representing the dipole as a consequence of its near field distortion by the particle. Thus a full physics electrodynamic model contains them automatically. However, in any such analysis we must keep in mind the comment by Dulkeith et al [1], that for a computed result to be rigorously compared to experiment, the statistical variations of the molecule's orientation and of its spectrum must be taken into account.

2.5 The electrodynamical viewpoints on fluorescence enhancement

Tam et al [46] have enumerated their requirements for a *complete* model of the interaction between a flurophore and a metal nanoparticle. It should include: (a) the hot spot phenomenon at the plasmon resonance, (b) quenching at contact between the molecule and the surface, (c) enhancement at a distance of a few nanometers, (d)

alteration of the quantum yield of the molecule and radiative decay rate, (e) the scattering efficiency of the metallic nanoparticle. All these features can be explained electrodynamically. The real question is, are the features properly combined in a *complete* model? If they were (for instance in the GN model) there should not be a two order of magnitude difference between prediction and experiment.

We propose that part of the problem lies in taking electrodynamical solutions piecemeal and then heuristically combining them to obtain the expectation. For instance, the hot spot phenomenon is often calculated by simply considering the metal nanoparticle in the presence of an incident plane wave, in the absence of the molecule. Under those conditions, (depending on the assumed loss in the particle) hundredfold and perhaps larger amplifications of the incident power density could be expected. This leads to the expectation that a hundredfold or larger increase in the excitation of the molecules located at the hot spot should occur. It never does. The reason is because omission of the molecule has invalidated that solution. As shown in [22] the scattering from the resonant molecule to the particle and back alters the total field at the molecule and leads to a dramatic reduction in the total power density available for excitation. The larger spontaneous emission from the absorption transition, the lower absorption/excitation enhancement we can get.

These results are not exactly new; it was contained in Das and Metiu's original model [13] and in its restating [14]. The omission of the molecule in much of the quenching vs. enhancement literature arises from mistaking an extinction cross section measurement of a given fluorophore in solution with the true resonant response of one individual molecule. The molecular spectrum measured in solution is a severely

inhomogeneously broadened spectrum (typical linewidth of 50nm in wavelength) leading to an apparent extinction cross section usually of the order of a tenth of a nanometer squared. In other words, the molecule is assumed to be a weak perturbation of the problem. However these spectra were statistical averaged and never separated this in-homogeneously broadened by environment apart. Hence these spectra could not demonstrate the individual molecule behavior in real. Each *individual* molecule's transition in reality has a spectrum with an ideal line-width of 10^{-3}nm from excited state lifetime (corresponding to an extinction cross section approximately $160{,}000nm^2$ and it should be homogeneously broadened by nonradiative transition to about 3 nm, corresponding to an extinction cross section of the order of $53nm^2$—which equals to the physical cross-section of 8nm sphere. Remember, experiments utilized 1.4nm gold sphere for the experiments. Even though the internal inversion would broaden the bandwidth homogeneous by thousand times, the individual molecule is as strong a scatterer as the nanoparticle and cannot be ignored.

A related misconception arises in the calculation of the fluorescence rate change (quantum yield change) expected when a molecule is placed in the presence of a resonant nanostructured environment. This appears in the literature as the photonic mode density effect. It is correctly stated that a complex environment (photonic band gap crystal, sub-wavelength cavities, and dielectric resonator) alters the photonic mode density of states available to a point radiator from what it normally has in free space [15]. As a result, the efficiency with which that radiator can release its energy can be dramatically altered. Since it has been known for a long time that electrodynamical calculations give exactly the same result as quantum mechanical ones [47] computational electromagnetics

methods have been used to calculate this effect [48, 49] in terms of the far field power density (or integrated total power) radiated by a unit current dipole. Comparing this power density in the two scenarios, presence and the absence of the nanostructure leads to the predicted rate change. However, we realized that not only the emission quantum yield, but also the absorption/excitation has to be considered.

In the next Chapter, we include all the above concerns into a full electrodynamical treatment of the fluorescence enhancement. By reviewing the three-level system diagram, we summarized the potential adjustable parameters in the system. In the end, the interactions between the molecule and the nanostructures would be understood, starting with the simple single sphere antenna. The backscattered by the nanostructures would be the key emphasis of the whole theory.

Chapter 3

QUANTUM-MECHANICAL DESCRIPTION ON THE FLUORESCENCE

In this chapter, we will review the quantum-mechanical description of the three-level system, and establish the relationship between the three-level system and the two-level system for absorption. The spontaneous emissions of from two excited states are treated separated, once the excitation/absorption and emission enhancements are separated. The total fluorescence enhancement is derived from the quantum mechanical description for the separation. The classic description of spontaneous emission is known as the dipole moment of a two-level system [50, 51]. We insert the dipole moment expression into the calculation on the local field calculation for the excitation/absorption. The difference against the simplified model would validate the existence of derating effects.

3.1 Three-Level system description

In Das and Metiu's papers [13, 14], they displayed a quantum-mechanical model of the molecule fluorescence rate. The considerations on both the spontaneous emission and the stimulated emission for both excitation and emission were implemented. For the low intensity illumination, we ignore the stimulated emission. Besides the emission quantum yield, the excitation quantum efficiency was also claimed to influence the fluorescence enhancement. The paper discussed the loss mechanism and radiation/scattering mechanism for the emission process. More importantly, it was claimed that the molecule's spontaneous emission A_{21} could provide an image field,

which shifts the absorption frequency level and the bandwidth. The effect was ignored since the image effect was thought as minor effects.

Since the illumination is always a narrow bandwidth around the exaction frequency ω_{21}, the interactions with other energy levels turn out to be trivial. Thus, the modeling generally treated the molecule as a three-level system with the excitation/absorbing frequency ω_{21}, and the emission frequency ω_{31}. In Fig.4, we re-plot the scheme for three-level system fluorescence, and we ignore the stimulated emission since we assumed that the incident wave was so weak that the induced emission is negligible. This assumption guarantees that the system is a linear time-invariant system. The incident photons first would be absorbed by the molecule, the electrons jump from Level I into Level II. Two possible decays happen simultaneously: the spontaneous emission A_{21} and the degeneration process K_{de} into a lower energy level III. The electrons would decay from Level III into the lower energy level I though both the radiative emission k_r and the non-radiative loss k_{nr}.

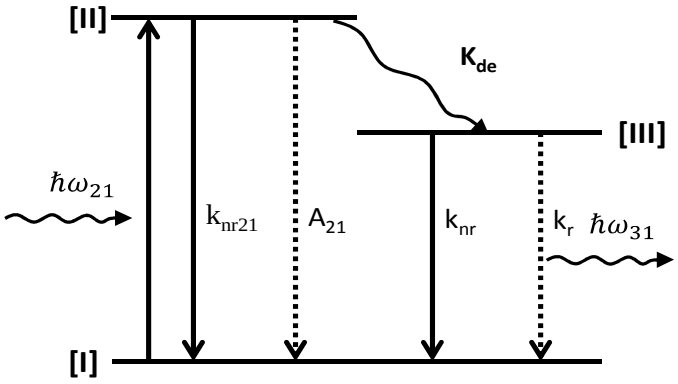

Fig. 3-1 Jacob Diagram for the three-level system

The equations of motions for the populations at three energy levels are written in the form of Einstein coefficients, non-radiative rates, and degeneration rate.

$$\begin{aligned}\dot{\mathrm{N}}_1 &= -\rho_\omega \mathrm{B}_{12}^{\omega}\mathrm{N}_1 + (\mathrm{A}_{21} + \mathrm{k}_{\mathrm{nr}21})\mathrm{N}_2 + (\mathrm{k}_{\mathrm{nr}} + \mathrm{k}_{\mathrm{r}})\mathrm{N}_3 \\ &= -\frac{\pi^2 \mathrm{c}^3}{\hbar\omega_{21}^3}\rho_{\omega_{21}}\mathrm{A}_{21}\mathrm{N}_1 + (\mathrm{A}_{21} + \mathrm{k}_{\mathrm{nr}21})\mathrm{N}_2 + (\mathrm{k}_{\mathrm{nr}} + \mathrm{k}_{\mathrm{r}})\mathrm{N}_3\end{aligned} \tag{3-1}$$

$$\dot{N}_2 = \rho_\omega B_{12}^{\omega} N_1 - (A_{21} + k_{nr21} + K_{de})N_2 \tag{3-2}$$

$$\dot{N}_3 = K_{de}N_2 - (k_{nr} + k_r)N_3 \tag{3-3}$$

The steady state solution requires $\dot{N}_1 = \dot{N}_2 = \dot{N}_3 = 0$. Since the incident light is weak, the population of level I N_1 should always near the total population N_0. The population of level II and III would be,

$$N_2 = \frac{\pi^2 c^3}{\hbar\omega_{21}^3}\rho_{\omega_{21}}\frac{A_{21}}{A_{21} + k_{nr21} + K_{de}}N_0 \tag{3-4}$$

$$N_3 = N_2\frac{K_{de}}{k_{nr} + k_r} = \frac{\pi^2 c^3}{\hbar\omega_{21}^3}\rho_{\omega_{21}}A_{21}\frac{K_{de}}{A_{21} + k_{nr21} + K_{de}}\frac{1}{k_{nr} + k_r}N_0 \tag{3-5}$$

The fluorescence rate can be calculated by multiplying the number density of level III and the radiative rate,

$$\gamma_{\mathrm{em}} = k_r N_3 = \frac{\pi^2 c^3}{\hbar\omega_{21}^3}\rho_{\omega_{21}}A_{21}\frac{K_{de}}{A_{21} + k_{nr21} + K_{de}}\frac{k_r}{k_{nr} + k_r}N_0 \tag{3-6}$$

In most cases, molecule has high degeneration rate, which mainly come from the vibrational relaxation process that fasten the decay by hundreds and thousands of times, especially for large molecules in solutions $K_{de} \gg A_{21} + k_{extra}$. Under this approximation, since $\rho_{\omega_{21}} \propto |\boldsymbol{\mu} \cdot \mathbf{E}_{\boldsymbol{local}}(\mathbf{r_m}, \omega)|^2$, the fluorescence enhancement is,

$$\frac{\gamma_{em}}{\gamma_{em\_0}} = \frac{\rho_{\omega_{21}}}{\rho_{\omega_{21\_0}}} \frac{QY}{QY_0} = \frac{\left|\boldsymbol{e_p} \cdot \boldsymbol{E}(\boldsymbol{r_m}, \omega)\right|^2}{\left|\boldsymbol{e_p} \cdot \boldsymbol{E_0}(\boldsymbol{r_m}, \omega)\right|^2} \cdot \frac{QY}{QY_0} \tag{3-7}$$

which is identical to the electromagnetic theory.

Even though we derived the identical Equations from the Quantum mechanics, we still miss the information on the local field adjustment by the molecule. The spontaneous emission A_{21} radiates the photon, and interacts with the sphere to scatter back on the molecule itself. The process could be taken into account by estimating the dipole moment of the molecule.

3.2 Two-Level system approximations and classic polarizability

When Das calculate the local field $\mathbf{E}_{\boldsymbol{local}}$, he not only considered the scattering field by reflection tensor $\mathbf{R}_{\boldsymbol{local}}(\omega)$, but also include the image tensor $\mathbf{G}(\omega)$ that represent the dipole image field from the sphere. Even though the image effect was not seriously considered in the previous analytical works, there are sufficient hints for molecular self-field interactions: the existence of the spontaneous emission was claimed to shift the center frequency for absorption. Interestingly, for the flat surface problem, Das did consider the image field in discussion [14]. The total field was separated into the primary field (incident field and its reflection field from the surface) and second field (self-image field and field from near fluorescent molecules). It was also claim that the secondary field has influence on the effective dipole polarizability, and in some situation, the scattering field might be stronger than the primary field. Few papers quantitatively calculated the secondary field influence in the absorption process. Here we will perform the analysis for

the single sphere enhancement for single molecule, and verify whether the secondary field is ignorable.

At the excitation frequency, the vibrational relaxation(degeneration) and decaying process in the emission could be consider as the “loss” energy, since it emission at another frequency incurs no coherence with the incident wave and the scattering wave. In that sense, the “loss” process contains the intrinsic loss in the molecule and the vibration relaxation, while we only deal with the excitation and emission between level II and level I. The excitation becomes a two-level system as shown below,

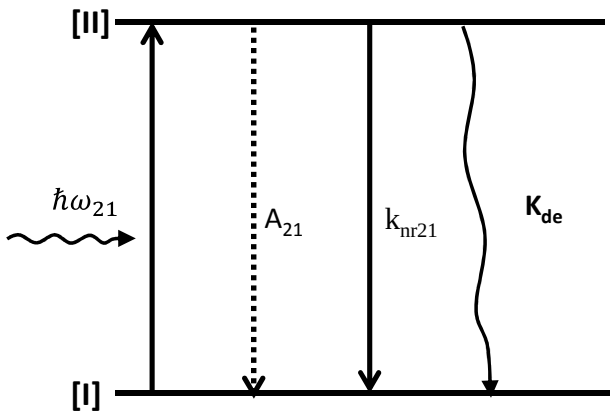

Fig. 3-2 Jacob Diagram for the equivalent two-level system

The spontaneous emission rate γ_{sca} scatters the partial power out of the molecule, which contributes to the scattering cross section of the molecule. The degeneration rate γ_{abs} calculated from Fig 5 could be easily written as,

$$\gamma_{\text{sca}} = A_{21}N_2 = \frac{\pi^2 c^3}{\hbar\omega_{21}^3}\rho_{\omega_{21}}\frac{K_{de}A_{21}^2}{A_{21}+K_{de}+k_{nr21}}N_0 \tag{3-8}$$

$$\gamma_{abs} = K_{de}N_2 = \frac{\pi^2 c^3}{\hbar\omega_{21}^3}\rho_{\omega_{21}}\frac{K_{de}A_{21}}{A_{21}+K_{de}+k_{nr21}}N_0 \tag{3-9}$$

Usually the degeneration rate K_{de} is much larger than the internal loss rate k_{nr21}, the absorption rate and emission rate could be simplified as,

$$\gamma_{\text{sca}} = A_{21}N_2 = \frac{\pi^2 c^3}{\hbar\omega_{21}^3}\rho_{\omega_{21}}\frac{K_{de}A_{21}^2}{A_{21}+K_{de}}N_0 \tag{3-10}$$

$$\gamma_{abs} = K_{de}N_2 = \frac{\pi^2 c^3}{\hbar\omega_{21}^3}\rho_{\omega_{21}}\frac{K_{de}A_{21}}{A_{21}+K_{de}}N_0 \tag{3-11}$$

The two-level system provide the same emission rate and loss rate as the three-level system, as long as we consider the fluorescence part as the loss for excitation frequency. When we model the excitation as such a simply system, it may not exhibit any fluorescence behavior from the absorption, but it indeed illustrates molecule spontaneous emission in the legitimate way.

Classically, such two-level system can be treated as a dipole antenna, or resonant linearly-polarized dipole. Thus, we could find the linear polarizability of a three-level system by utilizing the two-level system polarizability to solve the problem. In most papers and books, the complex polarizability of a two-level atom was generally written in one of the ways for calculations,

$$\boldsymbol{\alpha}(\omega) = \frac{{d_{21}}^2}{\hbar}\left(\frac{1}{\omega_{21}-\omega-i\gamma_{21}}+\frac{1}{\omega_{21}+\omega+i\gamma_{21}}\right)\mathbf{e}_p \tag{3-12}$$

where $\mathbf{e}_p$ is the linear polarization direction. d_{21} is the dipole moment, and γ_{21} is the total decay rate from Level II into level I, that is $A_{21}+K_{de}$. We assume that the decay rate is always much smaller than the resonant frequency, then the equation could be simplified by the definition the dipole moment of the two-level system.

(3-13)

(3-14)

The polarizability Equation (3-14) is legitimate, and it is consistent with the confined electron Lorentz model. The physical essence of the problem is that, the Two-level system molecule emission and absorption transitions are both considered as dipole resonant transitions, since the extremely small electrical size of the molecule limits its multi-pole radiation.

To demonstrate the physical meaning of this frequency dependent dipole moment in the classical electromagnetics, we find a corresponding antenna behaves the same way as a two-level system: one directional polarizability, same resonant frequency, same bandwidth and same extinction/scattering cross-section of certain two-level system molecule. The first trial is a short linear dipole antenna, with certain effective size. In the figure 6, we show the antenna with its circuit model.

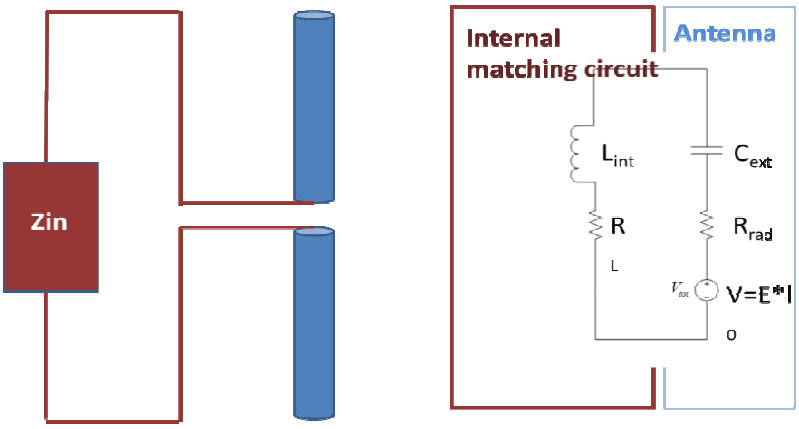

Fig. 3-3 Dipole and its corresponding equivalent circuit

From the antenna theory, we calculation the radiation resistance R_L from its effective size l_0; the external capacitance could be tuned by the radius of the wire [23]. In order to have the right resonant frequency, we need to insert corresponding inductance L_{int} in the internal matching network part as the modeling of molecule internal structure; the ratio of the decapitated power and re-radiated power (spontaneous emission), should be the ratio of the additional internal resistance R_L and the radiation resistance R_{rad}. Here is a table of all parameters of dipole antenna and two-level system parameters [23].

	Simplified two-level system	Short dipole antenna with LR matching network.
Absorption frequency	ω_{21}	$\sqrt{L_{int}C_{ext}}$
Extinction Cross section at the resonant frequency	$\frac{(3)\lambda^2}{2\pi}\frac{A_{21}}{A_{21}+k_{deg}}$	$\frac{3\lambda^2}{2\pi}\frac{R_{rad}}{R_{rad}+R_L}$
Scattering Cross section at the resonant frequency	$\frac{(3)\lambda^2}{2\pi}(\frac{A_{21}}{A_{21}+k_{deg}})^2$	$\frac{3\lambda^2}{2\pi}(\frac{R_{rad}}{R_{rad}+R_L})^2$
Scattering power/Loss power	$\frac{A_{21}}{A_{21}+k_{deg}}$	$\frac{R_{rad}}{R_{rad}+R_L}$
Bandwidth	$A_{21}+k_{deg}$	$\frac{R_{rad}+R_L}{L_{int}}$
polarizability	linear	linear
lineshape	lorenziation	lorenziation

Table 3-1 two-level sytem comparison with small dipole antenna

All the parameters could be identical, once we the circuit parameters satisfies the follow equations

$$R_L = \frac{k_{relax}}{A_{21}} R_{rad} \tag{3-15}$$

$$R_{rad} = L_{int} A_{21} \tag{3-16}$$

$$C_{ext} = L_{int} / \omega_{21}^2 \tag{3-17}$$

The only exceptions are the cross sections. That is because in the antenna calculation, it was always assumed that the polarization of the antenna is consistent with the polarization of the incident wave; the calculation for the cross section does not consider the situation that the antenna could be arbitrarily orientated, and 1/3 is the exact orientation factor which makes the cross sections identical.

The Three-level system was equivalent to the two-level system. The classical directional dipole moment of the two-level system was derived for calculate the absorption energy. Based on the dipole moment frequency dependency, we could provide an antenna with an intuitive view of the absorption mechanism of the molecules.

Chapter 4

THE EMISSION ENHANCEMENT BY SINGLE SPHERE

4.1 General Methods for calculating the emission modifications

The modification of quantum yield provides strong fluorescent enhancement/quenching effects in the molecular emission process. During the 1980s, several analytical theories based on classical electrodynamics for single molecule emission near a single sphere were published. Ruppin decomposed the emitting dipole into spherical harmonics, and solved the boundary condition problems using Mie theory [52, 18]. The resulting expression for the non-radiative loss on the sphere was an integral of spherical Hankel functions that requires numerical integrations. Gersten and Nitzan [17] published an electrostatic theory to calculate the radiative rate and non-radiative rate. Chew [16, 19] improved upon Ruppin's theory and re-calculated the total decay rate by using the electric field susceptibility. However, all these classical theories contains infinite sum of multipole terms. And the all these analytical methods could only be applied to the single molecule interaction with a single sphere. In 2005, Carminati and Greffet [21] proposed a simple method to model a metallic nano-particle as single dipole moment at the center of the sphere. The radiative rates and total decay rates are derived using a simple dipole-dipole coupling approach. However, this model has a limitation：

when the distance from emitter to the sphere gets closer than the radius, non-local effects would invalidate the dipole modeling for spheres.

Most theories assumed that the dipole moment of the molecule is not influenced by the environment. Hence we set the dipole moment as the constant $\boldsymbol{p_0}$. The problem becomes a discrete radiating dipole interacting with the sphere in the near distance. In the free space, the dipole moment provides the exact radiation power [23]:

$$P_{r0} = \frac{c^2 k^4}{12\pi} Z|\boldsymbol{p_0}|^2 \tag{4-1}$$

Hence, the radiative rate is,

$$\gamma_{r0} = \frac{P_{r0}}{\hbar\omega_{31}} \tag{4-2}$$

Suppose the dipole-behaved molecule has the intrinsic loss, we could define the internal loss rate as the non-radiative rate. The correlations between the intrinsic radiative rate γ_{r0}, the intrinsic non-radiative γ_{nr0}, the total decay rate γ_0 and the quantum yield QY_0 are shown as below,

$$QY_0 = \frac{\gamma_{r0}}{\gamma_0} \tag{4-3}$$

$$\gamma_0 = \gamma_{r0} + \gamma_{nr0} \tag{4-4}$$

We assumed that the intrinsic loss is not influenced by the electromagnetic environment changes. Therefore, the extra loss would be induced by the ohmic loss inside the sphere. The radiation power comes from the dipole radiation and the spherical wave scattering. With the vicinity of the sphere, the quantum yield would be modified,

$$QY = \frac{\gamma_r}{\gamma} \tag{4-5}$$

where both the radiative rate γ_r and the total decay rate γ are both modified.

$$\gamma_r = \frac{P_r}{\hbar\omega_{31}} \tag{4-6}$$

$$\gamma_{nr} = \frac{P_{nr0} + P_{nr\_sphere}}{\hbar\omega_{31}} = \gamma_{nr0} + \gamma_{nr\_s} \tag{4-7}$$

$$\gamma = \gamma_r + \gamma_{nr} \tag{4-8}$$

where we define γ_{nr_s} as the non-radiative rate induced by sphere. The sphere/dipole system is a linear system. So, we have the nonradiative rate induced by sphere and the raditiave rate proportional to the square of dipole moment.

4.2 Exact electrodynamical method

The exact electrodynamical method [19, 20] was most precise solution by classically electrodynamics. The arbitrary oriented molecule can be viewed as the superposition of a perpendicular dipole and a tangential dipole. Statistically, the arbitrarily oriented molecule has 1/3 perpendicular dipole moment and 2/3 tangential dipole moment. Hence, all the solutions separated the tangential dipole emission and the perpendicular dipole emission. Due to the symmetrical structure, we could always assume that the dipole is on the Z axis.

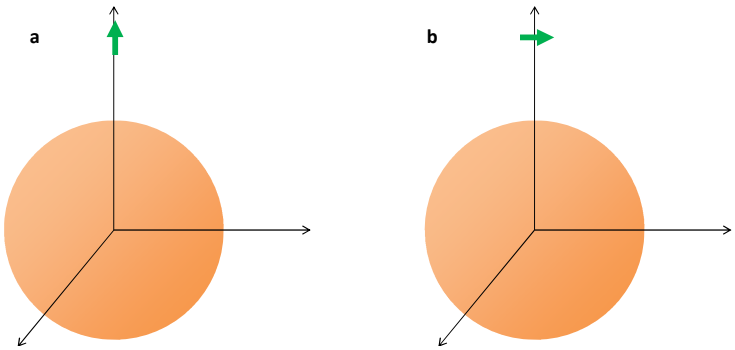

Fig. 4-1. Perpendicular dipole (a) and Tangential dipole emission (b) with the vicinity of the sphere

The off-centered dipole field could be viewed as the incident wave with the combination of infinite spherical harmonics [52]. In Fig. 4-1, we demonstrated that we separated the field into two parts: the inward field which requires finite field at the origin and the outward field propagating to the infinity. The electric field and the magnetic field are,

$$\boldsymbol{H}_{out} = \sum_{l,m} a_E(l,m) h_l^{(1)}(k_2 r) \boldsymbol{Y}_{llm} - \frac{i}{k_2} a_M(l,m) \nabla \times h_l^{(1)}(k_2 r) \boldsymbol{Y}_{llm} \tag{4-9}$$

$$\boldsymbol{E}_{out} = Z_2 \sum_{l,m} \frac{i}{k_2} a_E(l,m) \nabla \times h_l^{(1)}(k_2 r) \boldsymbol{Y}_{llm} + a_M(l,m) h_l^{(1)}(k_2 r) \boldsymbol{Y}_{llm} \tag{4-10}$$

$$\boldsymbol{H}_{in} = \sum_{l,m} \overline{a_E}(l,m) j_l\ (k_2 r) \boldsymbol{Y}_{llm} - \frac{i}{k_2} \overline{a_M}(l,m) \nabla \times j_l\ (k_2 r) \boldsymbol{Y}_{llm} \tag{4-11}$$

$$\boldsymbol{E}_{in} = Z_2 \sum_{l,m} \frac{i}{k_2} \overline{a_E}(l,m) \nabla \times j_l\ (k_2 r) \boldsymbol{Y}_{llm} + \overline{a_M}(l,m) j_l\ (k_2 r) \boldsymbol{Y}_{llm} \tag{4-12}$$

where k_2 is the wave number of in the space $\omega_{31}\sqrt{\varepsilon_2 \mu_2}$. Here we defined the orthonormal vector spherical harmonics as,

$$\boldsymbol{Y}_{llm} = \frac{1}{\sqrt{l(l+1)}} \boldsymbol{L} Y_{llm} = \frac{1}{\sqrt{l(l+1)}} \left(\frac{\boldsymbol{r} \times \boldsymbol{\nabla}}{i}\right) Y_{llm} \tag{4-13}$$

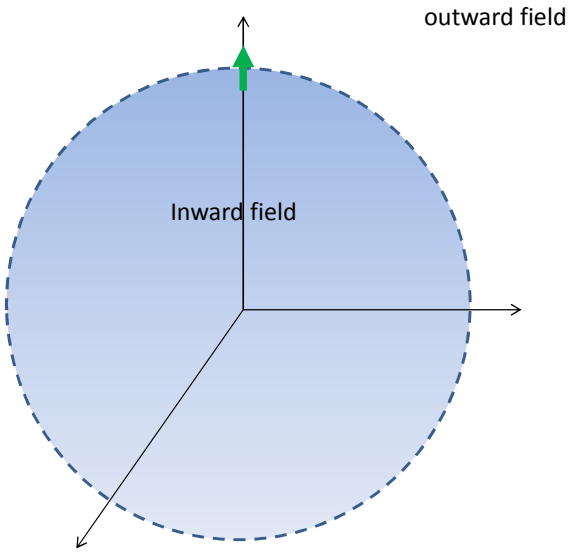

Fig. 4-2 off-centered Dipole field decomposition by spherical harmonics

The coefficients $a_E(l,m)$ and $a_M(l,m)$ specify the amount of different electric multipole and magnetics multipole fields. Once we know the electric current distribution and magnetic current distribution, we could figure out the expansion of the off-centered dipole field.

$$a_E(l,m) = \frac{k_2^2}{i\sqrt{l(l+1)}} \int Y_{llm}^* \begin{Bmatrix} c\rho \dfrac{\partial\left[k_2 r j_l\ (k_2 r)\right]}{\partial k_2 r} \\ +ik_2(\boldsymbol{r}\cdot\boldsymbol{J}) j_l\ (k_2 r) - ik_2 \nabla(\boldsymbol{r}\times\boldsymbol{M}) j_l\ (k_2 r) \end{Bmatrix} dxdydz \tag{4-14}$$

$$a_M(l,m) = \frac{k_2^2}{i\sqrt{l(l+1)}} \int Y_{llm}^* \begin{Bmatrix} \nabla(\boldsymbol{r}\times\boldsymbol{J}) j_l\ (k_2 r) + \boldsymbol{\nabla}\cdot\boldsymbol{M} \dfrac{\partial\left[k_2 r j_l\ (k_2 r)\right]}{\partial k_2 r} \\ -ik_2^2(\boldsymbol{r}\cdot\boldsymbol{M}) j_l\ (k_2 r) \end{Bmatrix} dxdydz \tag{4-15}$$

$$\overline{a_E}(l,m)$$

$$= \frac{k_2^2}{i\sqrt{l(l+1)}} \int Y_{llm}^* \begin{Bmatrix} c\rho \dfrac{\partial\left[k_2 r\, h_l^{(1)}(k_2 r).\right]}{\partial k_2 r} \\ +ik_2(\boldsymbol{r}\cdot\boldsymbol{J})\, h_l^{(1)}(k_2 r). - ik_2 \nabla(\boldsymbol{r}\times\boldsymbol{M})\, h_l^{(1)}(k_2 r). \end{Bmatrix} dxdydz \tag{4-16}$$

$$\overline{a_M}(l,m)$$

$$= \frac{k_2^2}{i\sqrt{l(l+1)}} \int Y_{llm}^* \begin{Bmatrix} \nabla(\boldsymbol{r}\times\boldsymbol{J}) h_l^{(1)}(k_2 r) + \boldsymbol{\nabla}\cdot\boldsymbol{M} \dfrac{\partial\left[k_2 r h_l^{(1)}(k_2 r)\right]}{\partial k_2 r} \\ -ik_2^2(\boldsymbol{r}\cdot\boldsymbol{M}) h_l^{(1)}(k_2 r) \end{Bmatrix} dxdydz \tag{4-17}$$

We could see that $\overline{a_E}$and $\overline{a_M}$ has the same formula as $a_E$and a_M except that the standing wave functions $j_l\ (k_2 r)$ are replaced by the traveling wave function $h_l^{(1)}(k_2 r)$.

Now, we us concentrate on the perpendicular dipole first. The dipole moment could be written as,

$$\boldsymbol{p_0} = \boldsymbol{e_r} p_0 \delta(\boldsymbol{r} - \boldsymbol{r'}) \tag{4-18}$$

where $\boldsymbol{r'}$ is the location of the dipole, and $\boldsymbol{r}$ is the observation point. The current density $\boldsymbol{J_r}$ could be related with $\boldsymbol{p_0}$ as,

$$\boldsymbol{J_r} = \frac{\omega_{31}}{i}\boldsymbol{p_0} = \frac{\omega_{31}}{i}\boldsymbol{e_r} p_0 \delta(\boldsymbol{r} - \boldsymbol{r'}) = \frac{\omega_{31}}{i}\boldsymbol{e_r} p_0 \frac{\delta(r - r')\delta(\cos\theta - 1)\delta(\varphi)}{r^2} \tag{4-19}$$

Therefore, the local charge distribution is ρ,

$$\rho_r = \frac{\mathbf{1}}{i\omega_{31}} \boldsymbol{\nabla}\cdot\boldsymbol{J_r} = -p_0 \frac{\delta(r - r')\delta(\cos\theta - 1)\delta(\varphi)}{r^2} \tag{4-20}$$

We also know that $\boldsymbol{r}\times\boldsymbol{J} = 0$ and $\boldsymbol{M} = 0$

$$\boldsymbol{r}\cdot\boldsymbol{J_r} = \frac{\omega_{31}}{i}\boldsymbol{e_r} p_0 \frac{\delta(r - r')\delta(\cos\theta - 1)\delta(\varphi)}{r} \tag{4-21}$$

Combing Equation (4-14)-(4-17) and Equation (4-19)- (4-21), we have

$$a_E(l,0) = \frac{\omega_{31} p_0}{i} k_2^2 \sqrt{l(l+1)\frac{2l+1}{4\pi}} \frac{j_l\ (k_2 d)}{(k_2 d)} \tag{4-22}$$

We also have $a_E(l,m) = 0\ ,\ when\ m \neq 0$, and $a_M(l,m) = 0$.

Hence, we this highly symmetrical structure, we do not have any magnetic multipole decompositions. All the φ-dependent terms are vanished.

The local field becomes,

$$\boldsymbol{H}_{out} = \sum_l a_E(l,0) h_l^{(1)}(k_2 r) \boldsymbol{Y}_{ll0} \tag{4-23}$$

$$\boldsymbol{E}_{out} = Z_2 \sum_l \frac{i}{k_2} a_E(l,0) \nabla \times h_l^{(1)}(k_2 r) \boldsymbol{Y}_{ll0} \tag{4-24}$$

$$\boldsymbol{H}_{in} = \sum_l \overline{a_E}(l,0) j_l\ (k_2 r) \boldsymbol{Y}_{ll0} \tag{4-25}$$

$$\boldsymbol{E}_{in} = Z_2 \sum_{l,m} \frac{i}{k_2} \overline{a_E}(l,0) \nabla \times j_l\ (k_2 r) \boldsymbol{Y}_{ll0} \tag{4-26}$$

By the Mie theory, the scattering field from the sphere is calculated term by term for each multipole component.

$$\boldsymbol{H}_{sca} = \sum_l B_l \overline{a_E}(l,0) h_l^{(1)}(k_2 r) \boldsymbol{Y}_{ll0} \tag{4-27}$$

$$\boldsymbol{E}_{sca} = Z_2 \sum_{l,m} \frac{i}{k_2} B_l \overline{a_E}(l,0) \nabla \times h_l^{(1)}(k_2 r) \boldsymbol{Y}_{ll0} \tag{4-28}$$

where B_l is the scattering coefficients for the electric multipole fields. We also have the magnetic multipole field scattering coefficients A_l from the Mie theory.

$$B_l = \frac{\varepsilon_2 j_l(k_2 a)[k_1 a j_l(k_1 a)]' - \varepsilon_1 j_l(k_1 a)[k_2 a j_l(k_2 a)]'}{\varepsilon_1 j_l(k_1 a)[k_2 a h_l^{(1)}(k_2 a)]' - \varepsilon_2 j_l(k_2 a)[k_1 a h_l^{(1)}(k_1 a)]'} \tag{4-29}$$

$$A_l = \frac{\mu_2 j_l(k_2 a)[k_1 a j_l(k_1 a)]' - \mu_1 j_l(k_1 a)[k_2 a j_l(k_2 a)]'}{\mu_1 j_l(k_1 a)[k_2 a h_l^{(1)}(k_2 a)]' - \mu_2 j_l(k_2 a)[k_1 a h_l^{(1)}(k_1 a)]'} \tag{4-30}$$

The total field and the back-scattered field onto the dipole is

$$\boldsymbol{E}_{tot} = \boldsymbol{E}_{sca} + \boldsymbol{E}_{out} = Z_2 \sum_{l,m} \frac{i}{k_2} [a_E(l,0) + B_l \overline{a_E}(l,0)] \nabla \times h_l^{(1)}(k_2 r) \boldsymbol{Y}_{ll0} \tag{4-31}$$

$$\boldsymbol{E}_{back} = \boldsymbol{E}_{sca}(\boldsymbol{r}') = Z_2 \sum_{l,m} \frac{i}{k_2} B_l \overline{a_E}(l,0) \nabla \times h_l^{(1)}(k_2 \boldsymbol{r}') \boldsymbol{Y}_{ll0}(0,0) \tag{4-32}$$

We simplify Equation (4-32) for the back-scattering field,

$$E_{back} = E_{sca}(r') = i\omega_{31} p_0 \frac{Z_2 k_2^2}{4\pi} \sum_l B_l (l+1) l (2l+1) \left(\frac{h_l^{(1)}(k_2 d)}{(k_2 d)}\right)^2 \tag{4-33}$$

The field would be used for the total decay rate and the absorption theory.

The radiative rate enhancement would be

$$\frac{\gamma_{r\_p}}{\gamma_{r0}} = \frac{P_{r\_p}}{P_{r0}} = \frac{3}{2} \sum_l l(l+1)(2l+1) \left| \frac{j_l\ (k_2 d)}{(k_2 d)} + B_l \frac{h_l^{(1)}(k_2 d)}{(k_2 d)} \right|^2 \tag{4-34}$$

The modification on the lifetime τ for fluorescence has been widely observed and analyzed by experiments, and the total decay rate is Γ defined as the inverse ratio of lifetime τ. From Chance, Prock and Silbey's work on the dipole interaction with a plane the expression of normalized total decay rate is calculated by the electric Green's function, which essentially calculates the back-scattered field from the environment (susceptibility) on the dipole itself when we set dipole moment as unity,

$$\begin{aligned} \frac{\gamma_p}{\gamma_{r0}} = \frac{P_p}{P_{r0}} &== 1 + \frac{6\pi\varepsilon_2}{k_2^3} \mathrm{Im}\left[\frac{E_{back}}{p_0}\right] \\ &= 1 + \frac{3}{2} \sum_l l(l+1)(2l+1) B_l \left(\frac{h_l^{(1)}(k_2 d)}{(k_2 d)}\right)^2 \end{aligned} \tag{4-35}$$

We could get the similar results for the tangential dipole field interaction with the sphere.

$$\boldsymbol{p_0} = \boldsymbol{e}_\theta p_0 \delta(\boldsymbol{r} - \boldsymbol{r}') \tag{4-36}$$

where $\boldsymbol{r}'$ is the location of the dipole, and $\boldsymbol{r}$ is the observation point. The current density $\boldsymbol{J_r}$ could be related with $\boldsymbol{p_0}$ as,

$$\boldsymbol{J}_\theta = \frac{\omega_{31}}{i}\boldsymbol{p_0} = \frac{\omega_{31}}{i}\boldsymbol{e}_\theta p_0 \delta(\boldsymbol{r} - \boldsymbol{r}') = \frac{\omega_{31}}{i}\boldsymbol{e}_\theta p_0 \frac{\delta(r - r')\delta(\theta)\delta(\varphi)}{r^2 \sin(\theta)} \tag{4-37}$$

Therefore, the local charge distribution is ρ,

$$\rho_\theta = \frac{1}{i\omega_{31}}\boldsymbol{\nabla} \cdot \boldsymbol{J}_\theta = -p_0 \frac{\delta(r - r')\delta(\theta)\delta(\varphi)}{r^2 \sin(\theta)} \tag{4-38}$$

We also know that $\boldsymbol{r} \cdot \boldsymbol{J_r} = 0$ and $\boldsymbol{M} = 0$.

$$\boldsymbol{\nabla} \cdot (\boldsymbol{r} \times \boldsymbol{J_r}) = \frac{\omega_{31}}{i} p_0 \frac{\delta(r - r')\delta(\theta)\delta'(\varphi)}{r^2 \sin(\theta)} \tag{4-39}$$

Combing Equation (4-14)-(4-17) and equation (4-37)-(4-39), we get the coefficients as,

$$a_E(l, \pm 1) = \pm \frac{\omega_{31} p_0}{2i} k_2^2 \sqrt{\frac{4\pi}{2l+1}} [(l+1) j_{l-1}(k_2 d) - l j_{l+1}(k_2 d)] \tag{4-40}$$

$$a_M(l, \pm 1) = \mp \frac{\omega_{31} p_0}{2i} k_2^2 \sqrt{\frac{2l+1}{4\pi}} j_l\ (k_2 d) \tag{4-41}$$

The normalized radiative rate the total rate are calculated as,

$$\frac{\gamma_{r\_t}}{\gamma_{r0}} = \frac{P_{r\_t}}{P_{r0}} = \frac{3}{4}\sum_l \begin{array}{c} (2l+1)\{\left| j_l\ (k_2 d) + A_l h_l^{(1)}(k_2 d) \right|^2 \\ + |[(k_2 d) j_l\ (k_2 d)]' + B_l \frac{[(k_2 d) h_l^{(1)}(k_2 d)]'}{(k_2 d)}|^2\} \end{array} \tag{4-42}$$

$$\frac{\gamma_t}{\gamma_{r0}} = \frac{P_t}{P_{r0}} = 1 + \frac{6\pi\varepsilon_2}{k_2^3}\mathrm{Im}\left[\frac{E_{back}}{p_0}\right]$$

$$= 1 + \frac{3}{4}\sum_l (2l+1)\{A_l[h_l^{(1)}(k_2 d)]^2 + B_l(\frac{[(k_2 d)h_l^{(1)}(k_2 d)]'}{(k_2 d)})^2\} \quad (4\text{-}43)$$

Here, we got the exact solution from the dipole/sphere interaction.

4.3 The Image model

In this part, we present a simple quasi-static model to describe the electromagnetic interaction between a dipolar emitting molecule and a Plasmonic (metal) nano-sphere. We approximate the effect of the Plasmonic nano-spheres on the molecule by replacing the sphere with off centered dipole images derived using the image theory of dielectric spheres. The retardation effect is taken into account by electrodynamical modifications on the spherical polarizability and the dipole radiation field. The modifications of the radiative rate, total decay rate and the quantum yield of a single molecule near the Plasmon sphere are also derived. The image model indicates strong distance dependence for the modification on the molecule's spontaneous radiative rates and total decay rates. Comparisons with the exact electrodynamical model and other simplified models indicate that the off-centered dipole images provide accurate predictions for the modified radiative rates and total decay rates, even at close distances. We propose a simplified model of Plasmon resonant sphere utilizing classical image theory. We start with the electrostatic image theory for metal spheres and dielectric spheres. We consider the electrodynamical effects of radiation damping and dynamical depolarization. The total decay rate is calculated from the electric-field susceptibility.

The spontaneous emission rate is calculated from the superposition of dipole moments. One important result is that the image theory not only accurately predicts the far field radiation, but also has fairly good approximation of the near field for the resonant sphere. We present the derivation of our dipole image model for the sphere, and the calculation of total decay rate and radiation rate based on dipole-dipole interaction. The numerical calculations for specific orientations of the molecular dipole would be performed. The comparison on the radiative rates, total decay rates and quantum yield would be derived. Based on the model, we summarize the results and draw conclusions.

First, we consider the emitting molecule or atom as an infinitesimally small radiating dipole with a constant dipole moment $\boldsymbol{p_0}$. We define the following basic parameters: the small dipole radiates at the frequency ω_0; the nano-sphere particle with the radius a is located at the origin of the Cartesian coordinate. The emitter dipole is assumed to be located at position $z=\boldsymbol{d}$ along z axis, and the distance between the emitter and the center of particle is $d=|\boldsymbol{d}|$. Two possible independent cases will be considered :(a) the dipole orientation is perpendicular to the sphere surface $\boldsymbol{p_{0\_z}}$; and (b) the molecular dipole orientation is parallel to sphere surface $\boldsymbol{p_{0\_x}}$.

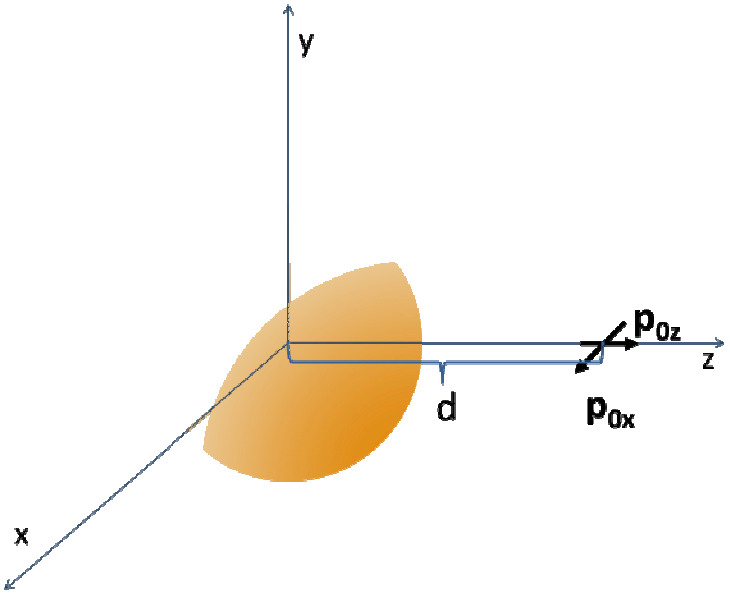

Fig. 4-3 Possible configuration of the dipole emitting near sphere

Electrostatically, a dipole emitter is usually treated as a positive charge and a negative charge - with finite distance . The small dipole assumption requires that the distance between point charges has to be much smaller than the radius of the sphere *a* and the distance from dipole to the origin *d*. The emitter's dipole moment is therefore . In Fig. 4-3, we illustrate the tangential and perpendicular image on the conducting sphere. For a single charge , two image charges are induced inside the PEC sphere. One charge is located at the center of the sphere, with charge quantity –. Another induced charge is located at , which is known as the Kelvin image [53, 54]. For the tangential dipole, the two source charges create two opposite charges at the center of the sphere. The total charge quantity at the center is — the net charge at the center becomes 0. The Kelvin images form a small dipole with the dipole moment — , located at the image point .

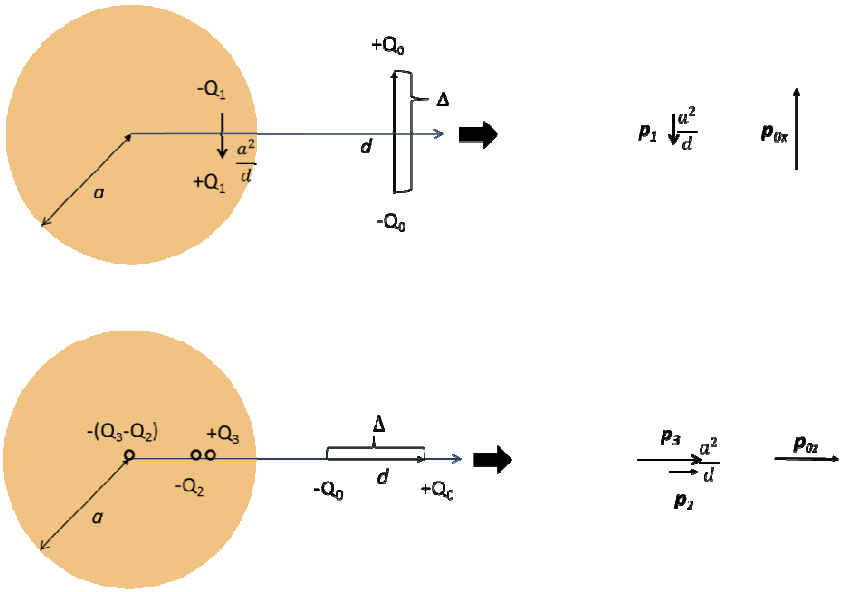

Fig. 4-4 Image of tangential and perpendicular dipole on a conducting sphere

For the perpendicular dipole, the image is more complicated: The negative charge induces an off-center charge ——, and the positive charge induces another off-center charge ——. Since the positive charge and the negative charge located at different distance with the sphere center, the net charge Q at the center is not 0 , ———. Thus, we separate the Positive charge into two parts to balance two negative charges as shown in the figure 2. Two dipoles are induced: a short dipole and a long dipole . The dipole moment could be calculated easily in equation 19 , when we assume .

— — — (4-44)

$$p_2 = Q_2\left(\frac{a^2}{d-\frac{\Delta}{2}} - \frac{a^2}{d+\frac{\Delta}{2}}\right) = Q_0\frac{a}{d+\Delta/2}\frac{a^2\Delta}{d^2-\Delta^2/4} \cong Q_0\Delta\frac{a^3}{d^3} = \frac{a^3}{d^3}p_0 \tag{4-45}$$

$$p_3 = Q_{cen}\frac{a}{d+\Delta/2} = Q_0\Delta\frac{a^2}{d^2-\Delta^2/4}\frac{a}{d+\Delta/2} \cong Q_0\Delta\frac{a^3}{d^3} = \frac{a^3}{d^3}p_0 \tag{4-46}$$

The classical image theory is not only generally applicable to perfect conducting spheres, but also applicable to the dielectric sphere [53, 54]: for the tangential dipole near dielectric sphere, the induced dipole moment could be modeled as an off-centered dipole located at the distance of a^2/d away from the origin. The perpendicular case the total dipole moment was spitted into two equivalent dipoles $\boldsymbol{p}_2$ and $\boldsymbol{p}_3$ at a^2/d and $a^2/2d$ for accuracy. The induced dipole $\boldsymbol{p}$ is proportional to the electric field on the dipole and the polarizability of the sphere.

$$\boldsymbol{p}_1 = \alpha\boldsymbol{E}_{\boldsymbol{x}}\delta(\mathrm{z}-\frac{a^2}{d}) \tag{4-47}$$

$$\boldsymbol{p}_2 = \frac{1}{2}\alpha\boldsymbol{E}_{\boldsymbol{z}}\delta(\mathrm{z}-\frac{a^2}{d}) \tag{4-48}$$

$$\boldsymbol{p}_3 = \frac{1}{2}\alpha\boldsymbol{E}_{\boldsymbol{z}}\delta(\mathrm{z}-\frac{a^2}{2d}) \tag{4-49}$$

In the electrostatic limit, the expression of polarizability α_0 and driven electric fields $\boldsymbol{E}$ generated from dipole source could be written as

$$\alpha_0 = 4\pi\varepsilon_2 a^3\frac{\varepsilon_1-\varepsilon_2}{\varepsilon_1+2\varepsilon_2} \tag{4-50}$$

$$\boldsymbol{E}_z = 2\boldsymbol{p}_{0z}/(4\pi\varepsilon_2 d^3) \tag{4-51}$$

$$\boldsymbol{E}_x = -\boldsymbol{p}_{0x}/(4\pi\varepsilon_2 d^3) \tag{4-52}$$

where p_0 is the dipole moment of the emitter, the subscripts z and x represent the orientation, and ε_2 is the permittivity of the surrounding medium, usually free space or water solution. If we set the sphere as a perfect electric conductor, the permittivity of the sphere $\varepsilon_1 = 1 + \infty \cdot i$, we would result in the exact dipole moment shown in Equation (4-47)-(4-49).

To accurately calculate the total radiation rate and decay rate, several adjustment are made for the calculation: the dipole field has to take the radiation terms into account; the polarizability has to account for radiation damping and dynamic depolarization as shown in the Equation (4-53)-(4-55),

$$\alpha_d = \frac{\alpha_0}{1 - \frac{ik_2^3\alpha_0}{6\pi} - \frac{k_2^2\alpha_0}{6\pi a}} \tag{4-53}$$

$$\boldsymbol{E}_{zd} = 2\boldsymbol{p}_{0z}\frac{1}{4\pi\varepsilon_2}\left(\frac{1}{d^3} - \frac{ik_2}{d^2}\right) \tag{4-54}$$

$$\boldsymbol{E}_{xd} = \boldsymbol{p}_{0x}\frac{1}{4\pi\varepsilon_2}\left(\frac{ik_2^2}{d} + \frac{ik_2}{d^2} - \frac{1}{d^3}\right) \tag{4-55}$$

where k_2 is the wave number The expressions of the induced dipole moment is,

$$\boldsymbol{p}_1 = \alpha_d \boldsymbol{E}_{xd}\delta\left(\mathrm{z} - \frac{a^2}{d}\right)) \tag{4-56}$$

$$\boldsymbol{p}_2 = \frac{1}{2}\alpha_d \boldsymbol{E}_{zd}\delta\left(\mathrm{z} - \frac{a^2}{d}\right) \tag{4-57}$$

$$\boldsymbol{p}_3 = \frac{1}{2}\alpha_d \boldsymbol{E}_{zd}\delta(\mathrm{z} - \frac{a^2}{2d}) \tag{4-58}$$

4.4 The total decay rate and the radiative rate by image dipole theory

The back-scattered fields by the perpendicular and tangential dipoles are all due to the induced dipole. Combining Equations (4-53)-(4-58) ,and we apply the location of the induced dipole: $\boldsymbol{p_1}$ and $\boldsymbol{p_2}$ are located at a^2/d away from the origin along z axis; $\boldsymbol{p_3}$ is located at $a^2/2d$ away from the origin along z axis. Hence, the distance from the image $\boldsymbol{p_1}$ and $\boldsymbol{p_2}$ to the radiating dipole is $d_2 = d - a^2/d$; the distance from the image dipole to the radiating dipole is $d_3 = d - a^2/2d$.The expression for the backscattered field S^b of unit dipole is written as,

$$S^b_{\tan} = \frac{\alpha}{4\pi\varepsilon_2}(\frac{ik_2^2}{d} + \frac{ik_2}{d^2} - \frac{1}{d^3})\frac{1}{4\pi\varepsilon_2}(\frac{ik_2^2}{d_2} + \frac{ik_2}{d_2^2} - \frac{1}{d_2^3}) \tag{4-59}$$

$$S^b_{\mathrm{per}} = \frac{\alpha}{4\pi\varepsilon_2}\left(\frac{1}{d^3} - \frac{ik_2}{d^2}\right)\frac{1}{2\pi\varepsilon_2}[\left(\frac{1}{d_2^3} - \frac{ik_2}{d_2^2}\right) + \left(\frac{1}{d_3^3} - \frac{ik_2}{d_3^2}\right)] \tag{4-60}$$

The expression for the total decay rate of the tangential and perpendicular dipole are simply written as,

$$\frac{\gamma_t}{\gamma_{r\_0}} = 1 + \frac{6\pi\varepsilon_2}{k_2^3}\mathrm{Im}(S^b_{\tan}) \tag{4-61}$$

$$\frac{\gamma_p}{\gamma_{r\_0}} = 1 + \frac{6\pi\varepsilon_2}{k_2^3}\mathrm{Im}(S^b_{\mathrm{per}}) \tag{4-62}$$

Once we assume that it is in near distance, the dipole radiation the superposition of the emitter dipole and the induced dipole fields. The simple expressions of the normalized radiative rates γ_r are therefore:

$$\frac{\gamma_{r\_t}}{\gamma_{r\_0}} = \frac{|\boldsymbol{p}_0 + \boldsymbol{p}_1|^2}{|\boldsymbol{p}_0|^2} = |1 + \alpha \frac{1}{4\pi\varepsilon_2}(\frac{ik_2^2}{d} + \frac{ik_2}{d^2} - \frac{1}{d^3})|^2 \tag{4-63}$$

$$\frac{\gamma_{r\_p}}{\gamma_{r\_0}} = \frac{|\boldsymbol{p}_0 + \boldsymbol{p}_1 + \boldsymbol{p}_2|^2}{|\boldsymbol{p}_0|^2} = |1 + \alpha \frac{1}{2\pi\varepsilon_2}(\frac{1}{d^3} - \frac{ik_2}{d^2})|^2 \tag{4-64}$$

The extra non-radiative rate that account for the loss in the sphere is calculated by the total decay rate minus the radiative rate.

$$\gamma_{nr} = \gamma \quad - \gamma_r \tag{4-65}$$

4.5 Numerical comparisons against classical EM models

To verify the image model for near field dipole-sphere interactions, we calculate the total decay rate and the radiative rate for a few specific situations. Consider an emitter radiating at Silver nano-particle's plasmon resonant frequency in free space — 354nm. We take the value of Silver's dielectric constant as $\varepsilon_1(354nm) = -2.03 + 0.6i$ from [55]. We choose a 30nm Silver diameter sphere as an example of an electrically small Plasmon nano-sphere.

In Fig. 4-5, we show a comparison between the distance-dependent total decay rates and radiative rates by the image model (magenta dashed lines), the exact electrodynamical theory (red solid lines), GN models (Blue solid lines) and Carminati/Greffret's model (Brown solid lines). The tangential (Fig. 4-5 (a-b)) and perpendicular (Fig. 4-5(c-d)) orientations are considered separately. In Fig. 4-5(a) and (c), we concentrated on the total decay rate modifications: Both the image model and GN model have fairly good match with the exact theory for both orientations. Caminati/Greffet's mothod has good estimations until the distance gets below 15nm where the model leads to a substantial underestimation of the total decay rates. Both the

image theory and Caminiati's dipole theory are based on the near field calculation of susceptibility. The deviation indicates that the equivalent induced dipole position should be located off-center instead of being centered for the near-field interaction between the dipole and the plasmon sphere. In addition, we could still observe some deviation from the image theory. This is because the actual dielectric sphere image is not a point dipole, but rather a continuous dipole distribution along the axis. At close distances, errors due to phase and the back-scattered fields by the point dipole image calculations increase and contribute to the discrepancy.

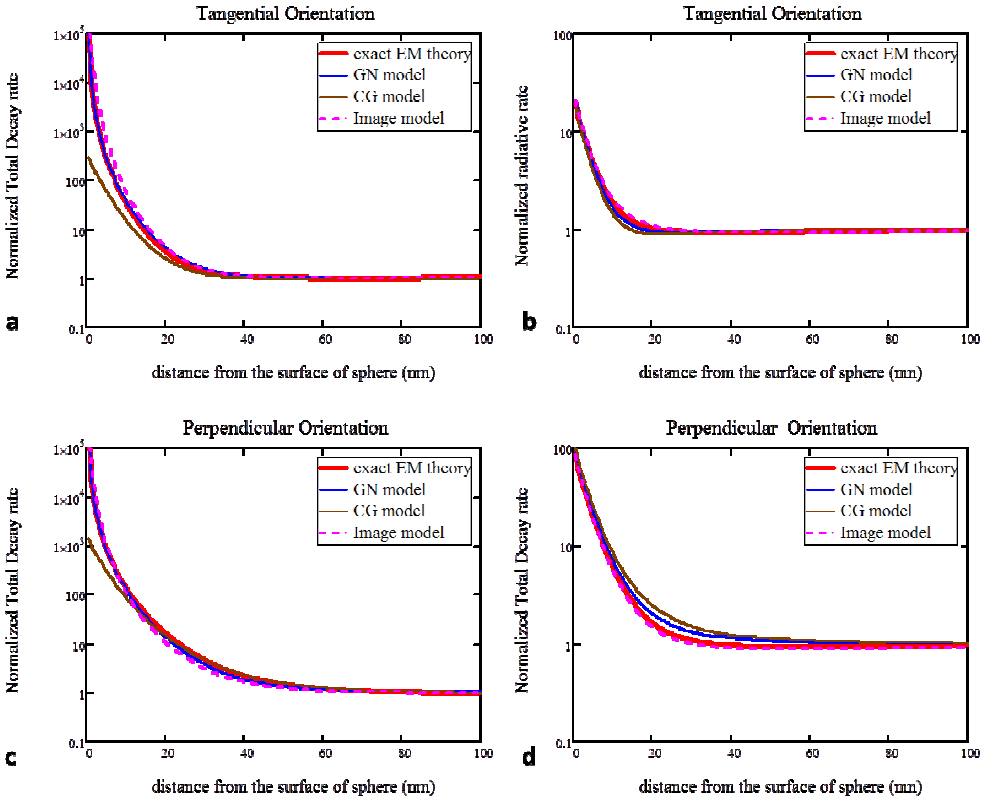

Fig. 4-5 Total decay rates and radiative rates by d=30nm sphere

In Fig. 4-5, we show a comparison between the distance-dependent total decay rates and radiative rates by the image model (magenta dashed lines), the exact electrodynamical theory (red solid lines), GN models (Blue solid lines) and Carminati/Greffret's model (Brown solid lines). The tangential (Fig. 4-5 (a-b)) and perpendicular (Fig. 4-5(c-d)) orientations are considered separately. In Fig. 4-5(a) and (c), we concentrated on the total decay rate modifications: Both the image model and GN model have fairly good match with the exact theory for both orientations. Caminati/Greffet's mothod has good estimations until the distance gets below 15nm where the model leads to a substantial underestimation of the total decay rates. Both the image theory and Caminiati's dipole theory are based on the near field calculation of susceptibility. The deviation indicates that the equivalent induced dipole position should be located off-center instead of being centered for the near-field interaction between the dipole and the plasmon sphere. In addition, we could still observe some deviation from the image theory. This is because the actual dielectric sphere image is not a point dipole, but rather a continuous dipole distribution along the axis. At close distances, errors due to phase and the back-scattered fields by the point dipole image calculations increase and contribute to the discrepancy.

Fig. 4-5(b) and (d) describes the radiative rate modification by a plasmonic sphere. We found that the image theory provides a more accurate description of the modified molecular emission compared to the GN model and Carminati/Greffet's model. The improvement is due to the modification of the sphere's polarizability with dynamic terms shown in Eq. (4-53), where the phase delay and sphere radiation was accounted for. For the tangential orientation, the GN model and the Carminati/Greffet model

underestimated the total radiation, whereas they would overestimate the total radiation for the perpendicular orientation. The point image approximation has little influence when we calculate the far field radiation. That is why the radiative rates are consistent with the exact electromagnetic theory. However, the total decay rate calculation involves near field calculations, which leads to the deviation between the point dipole approximations against the realistic current distribution in the sphere.

The quantum yield modification is an important consideration for fluorescence enhancement/quenching. In most fluorescence experiments, an emitter radiating near a plasmon sphere would be quenched or enhance med depending on the emitter quantum yield. We consider two different kinds of molecules: a 100% intrinsic quantum yield molecule and a 1% low quantum yield molecule and subsequently demonstrate the calculations from different models.

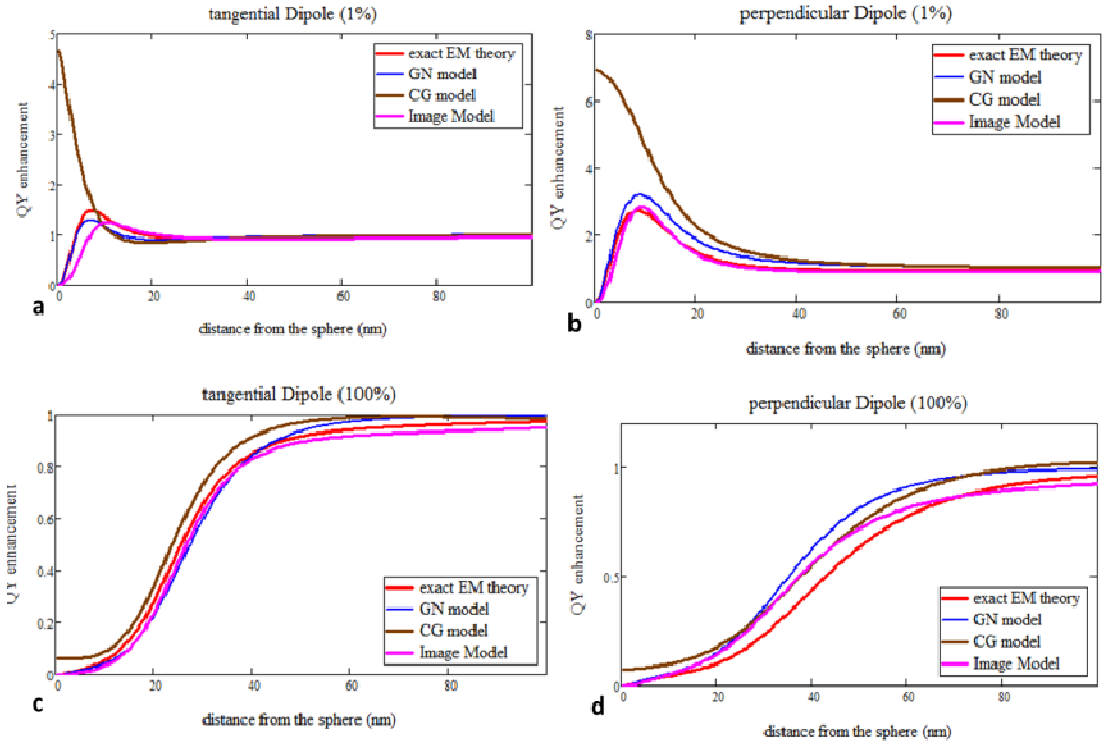

Fig. 4-6 Quantum yield of 100% and 1% molecule by d=30nm sphere

In Fig. 4-6, we show the quantum yield enhancement for QY_0=100% and 1%. In Fig. 4-6(a) and Fig. 4-6(b), the enhancement estimated by the image model has very good agreement for 1% intrinsic quantum yield molecule. For the tangential dipole, the optimal enhancement distance predicted by the image theory was 2nm longer than the exact optimal distance. The Carminati/Greffet's model overestimated the maximum enhancement by three times， and the optimal distance for enhancement is not predicted. For the perpendicular orientation, the image model almost overlaps with the exact electrodynamical: both of them predict 2.6 times enhancement at 9nm away from the sphere. GN model has little deviation on the enhancement factor and optimal distance. Image theory still overestimated the enhancement and predicted no optimal distance for the enhancement. In Fig. 4-6(c) and (d), we show the quenching effects on the 100% quantum yield dipole near a plasmon sphere. All the models predicted huge quenching when the emitter gets close the sphere. Still, the Image method provides the closest prediction against other theories.

To observing the advantage of the image theory, we also compare the total decay rate, the radiative rate, and the quantum yield enhancement of the molecule with the vincity of a large sphere with 60nm diameter.

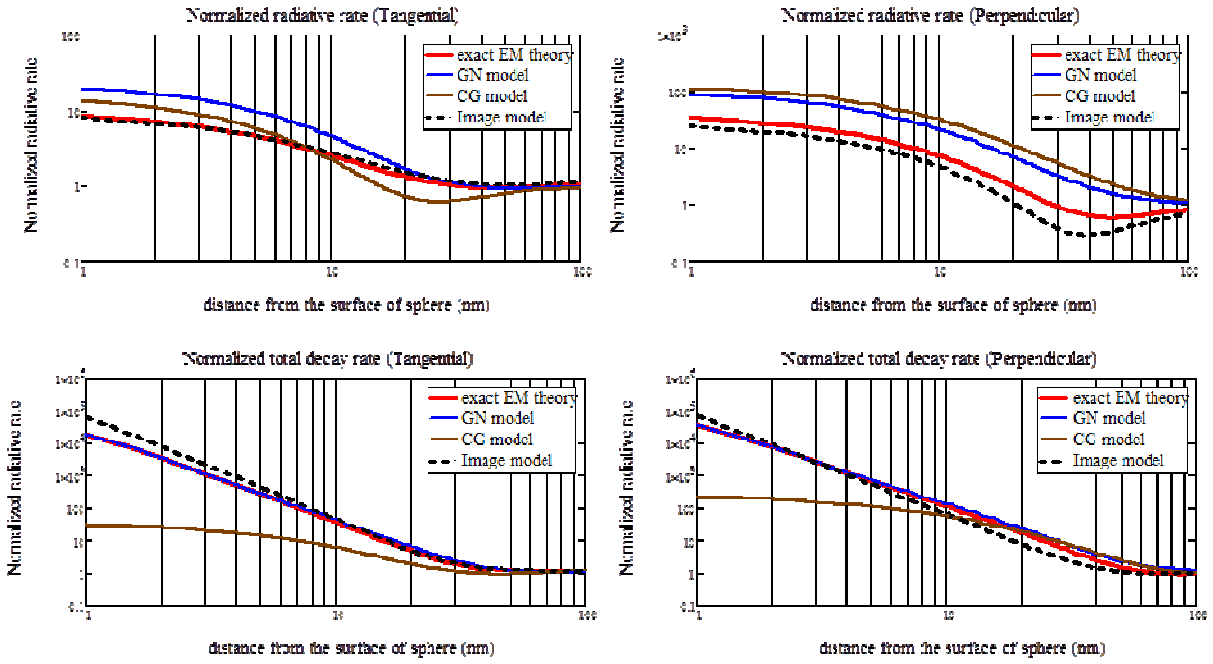

Fig. 4-7 Total decay rates and radiative rates by d=60nm sphere

In Fig. 4-6, we still find that the image theory model provide accurate results on the radiative rate, while GN model overestimate the rates over 3 times in the near distance for both the tangential and perpendicular dipole case. Even though there is small deviation on the total decay rate, the image theory still provide accurate prediction on the quantum yield enhancement factor and the optimum distance for both orientations.

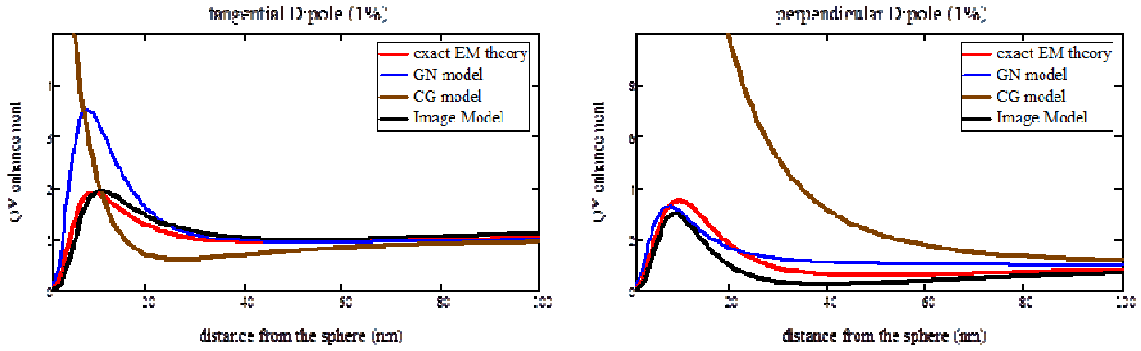

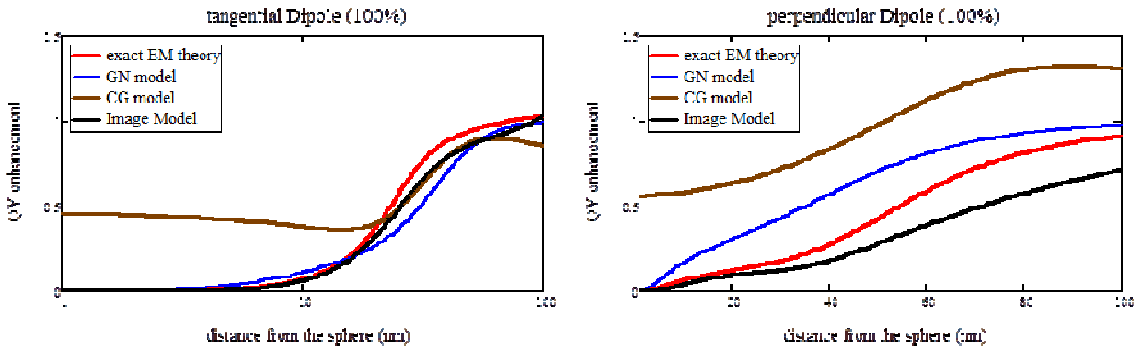

Fig. 4-8 Quantum yield enhancement of 100% and 1% molecule by d=60nm sphere

4.6 Conclusions

In this chapter, we first we derived the spontaneous decay rates and radiative rates of a single dipole near a single plasmonic metal nano-particle based on classical electrodynamical theory. The normalized total decay rates and radiative rates consist of an infinite sum of multipole terms. The image theory provides simple forms for radiative rate, the total decay rate and the quantum yield enhancement factor. The comparison with different models demonstrated the following conclusions for the Plasmonic sphere interaction with the discrete dipole: (1) Image theory requires an off-centered dipole image to model the scattering of dielectric field accurately. (2) The total modified decay rates and modified radiative rates calculated by image theory provide better consistency with exact electrodynamical theory. (3) The image method could accurately predict the quantum yield enhancement factor and optimal conditions for emitters near plasmonic spheres. (4) For large size spheres, the image theory demonstrated better prediction on the quantum yields enhancement than the Gersten-Nitzan model. Note that for the total fluorescence enhancement calculation in the following chapters, we will still use the electrodynamical theory for accuracy.

Chapter 5

THE EXACT ELECTRODYNAMICAL TREATMENT AND SOLUTIONS FOR EXCITATION/ABSORPTION ENHANCEMENT

5.1 Introduction

The fluorescence enhancement by a single Plasmon sphere is separated into excitation/absorption enhancement K_{exc} and the emission quantum yield enhancement K_{em}. Incorporating the classical model of molecular spontaneous emission into the excitation/absorption transition, the excitation enhancement is calculated rigorously by electrodynamics in the frequency domain. The final formula for the excitation enhancement contains two parts: the primary field enhancement calculated from the Mie theory, and a derating factor due to the backscattering field from the molecule. The enhancement factor for an arbitrarily located and randomly oriented molecule is separated into the tangential dipole case and the perpendicular dipole case. The primary field enhancement requires a solid angular average for both orientations. When compared against a simplified model that only involves the Mie theory field calculation, this more rigorous model indicates that under monochromatic (resonant) illumination, the excitation enhancement near the surface of the sphere is quenched severely due to the back-scattering field from the molecule. By sweeping the incident wavelength, we investigate the frequency red-shift and bandwidth broadening in the absorption spectra. For the more realistic broadband illumination scenario, we calculate the final enhancement by integrating over the excitation/absorption spectrum. The numerical results indicate that the resonant illumination scenario would underestimate the

total excitation enhancement if the illumination has a broader bandwidth than the molecule. Combining with the exact Electrodynamical theory for emission, the realistic model demonstrates that there is a potential for significant fluorescence enhancement for the case of a low quantum yield molecule close to the surface of the sphere. For example at 5 to 10nm from a 15nm Ag sphere, a 1% QY molecule could experience a total enhancement factor of 137.

The modification of quantum yield K_{em} by a single sphere was deeply investigated theoretically during the 1980s based on classical electrodynamics. Ruppin decomposed the emitting dipole into spherical harmonics, and solved the boundary condition problem using the spherical harmonics [18]. The resulting expression for the non-radiative loss on the sphere was obtained as an integral of spherical Hankel functions that requires numerical integrations. Gersten and Nitzan [17] published an electrostatic theory to calculate the radiative rate and non-radiative rate in a simpler form. The Gersten/Nitzan (GN) model is widely used for comparison with experimental results. Chew [19, 20] improved upon Ruppin's theory and re-calculated the total decay rate by using the electric field susceptibility. Chew's method has been widely used and has been called the exact electrodynamical method since it provides the most accurate Green's function solution from the Electromagnetic viewpoint. There have been proposals to reduce Chew's result into simpler expressions [21, 44] but in its original form Chew's approach is the most accurate electromagnetic treatment.

While the emission theory has been well developed, the other important modification for fluorescence, namely the excitation modification, has been treated in an extremely simple way: the modified local field $\boldsymbol{E_{tot}}$ is just calculated as the sum of the

incident wave $\boldsymbol{E_{inc}}$ and the scattered field $\boldsymbol{E_{sca}}$ from the sphere. The expressions for the scattered field are easily obtained from Mie Theory [7, 56]. The molecule's existence and its self-electromagnetic-interaction with the sphere are usually not considered for excitation. Yet, in the case of Raman Surface Enhancement [29, 30] the resonant molecular field is acknowledged to highly influence the local field and excitation enhancement. Since the fluorescence enhancement calculation can be shown to be analogous to the Raman enhancement calculation, the molecule interaction effects should not be ignored.

Even though it is true that the emission light at frequency ω_{31} has no coherency with the incident light because the degeneration process is so fast, this is not true of the "weak" spontaneous emission at the frequency ω_{21}. This radiation emitted during the absorption process must be taken into account for accurate modeling from the Electromagnetic aspects. Only then can it be determined if this term is a slight perturbation or a significant effect.

To investigate the problem, we organize this paper in the following way: we start with the quantum mechanical description of the fluorescence molecules. Similar to the published emission theories, we assume the molecular dipole induced during excitation is infinitesimally small. We take the molecular radiation field (spontaneous emission) into account when we compare the total field with the simple Mie theory results for monochromatic illumination. Strong interactions between the molecule's near field and the sphere induce an excitation frequency shift. Hence, it is necessary to perform the spectrum integral for realistic excitation enhancement. Combining with the emission

theory, we observe the effects on the total fluorescence enhancement factor and determine optimum distances for the same.

5.2 Polarizability and secondary field from re-radiation

A quantum-mechanical model of the molecule fluorescence rate modification by a single small sphere was developed by Das and Metiu [13]. Rather than being limited to small spheres, we extend our applications to arbitrary size spheres. To utilize the classical electromagnetic theories, we need to turn the related quantum-mechanical terms into the classical descriptions [13]. We start with plotting the scheme for three-level system fluorescence in, and we ignore the stimulated emission since we assumed that the incident wave was so weak that the induced emission is negligible. This assumption guarantees that the system is a linear time-invariant system. The incident photons are first absorbed by the molecule, the electrons promoted from Level I into Level II. Two possible decays can happen simultaneously: the spontaneous emission A_{21} and the degeneration process K_{de} into a lower energy level III. The electrons then decay from Level III into the lower energy level I though both the non-radiative loss k_{nr} and the radiative emission k_r, which turns out to be the fluorescence emission.

Most important in this Jacob diagram is the fact that even though most electrons in state II would degenerate into state III, the spontaneous emission always happens. In the development that will follow it will be shown that for the case of excitation enhancement, the molecule's spontaneous emission A_{21} induces a dipole in the nanosphere (an "image") whose re-radiated field interferes with the total incident (Mie solution) field. Additionally, this effect shifts the absorption frequency level and alters its

bandwidth. This component of the excitation has been routinely ignored in the literature by claiming that it is a minor perturbation.

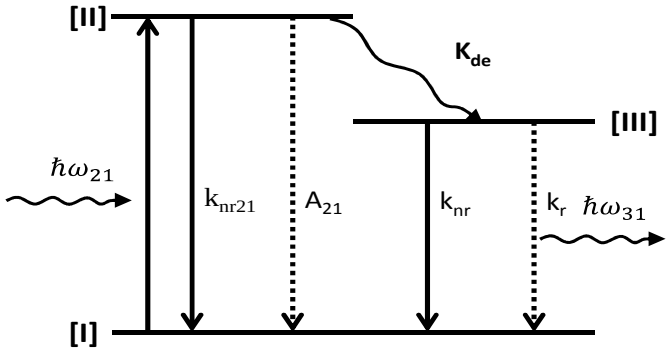

Fig. 5-1 Jacob Diagram for the three-level system

Instead of using quantum mechanics, we consider the coherent scattering/re-radiation field A_{21} in classical electrodynamics. Since it is well known that resonant electrically small antennas scatter as much energy as they absorb, it becomes clear that the presence of the molecule cannot just be a perturbation. The quantum self-radiation behavior of transition from state II into I is described by the linear polarizability $\boldsymbol{\alpha}(\omega)$, which is given in Equation (5-1) [50, 51].**Error! Reference source not found.**

$$\boldsymbol{\alpha}(\omega) = \frac{{d_{21}}^2}{\hbar}\left(\frac{1}{\omega_{21} - \omega - i\gamma_{21}} + \frac{1}{\omega_{21} + \omega + i\gamma_{21}}\right)\mathbf{e}_p \tag{5-1}$$

where $\mathbf{e}_d$ is the absorption dipolar transition polarized direction. d_{21} is defined as the dipole moment for the absorption transition, and γ_{21} is the total decay rate from Level II into level I, that is $A_{21} + K_{de}$. We assume that the decay rate is always much smaller than the resonant frequency. The dipole moment is related to the spontaneous emission rate A_{21}. Hence, the polarizability could be simplified as follows.

$$d_{21}{}^{2} = \frac{6\pi\varepsilon_0\hbar c^3}{\omega_{21}^3} A_{21} \tag{5-2}$$

$$\boldsymbol{\alpha}(\omega) = \frac{3\lambda_0^2}{2\pi \cdot Z_0} \frac{A_{21}}{\omega_{21}^2 - \omega^2 - i(A_{21} + k_{de})\omega} \mathbf{e}_p \tag{5-3}$$

The coefficient $\gamma_{21}(\omega)$ was approximated as $\gamma_{21}(\omega_{21})$ because the single molecule has an extremely narrow absorption band. We do have another assumption here: the molecule excitation/absorption transition is linearly polarized. We could use the tensor polarizability for the more general case. For this session, we apply the simple form of equation to investigate the secondary field effect.

5.3 Separation on Primary field (Mie Field) and secondary field effect

The total local field is the key to modeling the excitation enhancement. Instead of the oversimplified model, which only calculates the incident field and the scattered field from the sphere, we add the addition secondary field $\boldsymbol{E_{sec}}$ that includes the molecular spontaneous emission as shown in Fig. 5-2. The dipole emission field interacts with the sphere that in turn backscatters the secondary field $\boldsymbol{E}_{sec}$ onto the molecule itself. Obviously, the dipole strength $\boldsymbol{p}$ affects the backscattering field and the total local field around the molecule itself.

The local field is first written in the frequency domain, as the sum of primary Mie field $\boldsymbol{E}_p(\omega, \boldsymbol{r_m})$ and the secondary field $\boldsymbol{E}_{sec}(\boldsymbol{r_m}, \omega)$, at the location of the molecule

$$\boldsymbol{E}_{tot}(\omega, \boldsymbol{r_m}) = \boldsymbol{E}_p(\omega, \boldsymbol{r_m}) + \boldsymbol{E}_s(\omega, \boldsymbol{r_m}) \tag{5-4}$$

where ω is the frequency we interested in, and $\boldsymbol{r_m}$ is the position of the dipolar molecule with the excitation model. The dipole moment is related to the local field

$\boldsymbol{E}_{tot}(\omega, \boldsymbol{r}')$ and the polarizability $\boldsymbol{\alpha}(\omega)$. Note that bother parameters are frequency dependent.

The dipole moment is related to the local field $\boldsymbol{E}_{tot}(\boldsymbol{r}_{\boldsymbol{m}}, \omega)$ and the polarizability $\boldsymbol{\alpha}(\omega)$. Note that both parameters are frequency dependent.

$$\boldsymbol{p}(\omega) = [\boldsymbol{\alpha}(\omega) \cdot \boldsymbol{E}(\omega, \boldsymbol{r}_{\boldsymbol{m}})]\boldsymbol{e}_p = [\boldsymbol{\alpha}(\omega) \cdot (\boldsymbol{E}_p(\omega, \boldsymbol{r}_{\boldsymbol{m}}) + \boldsymbol{E}_s(\omega, \boldsymbol{r}_{\boldsymbol{m}}))]\boldsymbol{e}_p \tag{5-5}$$

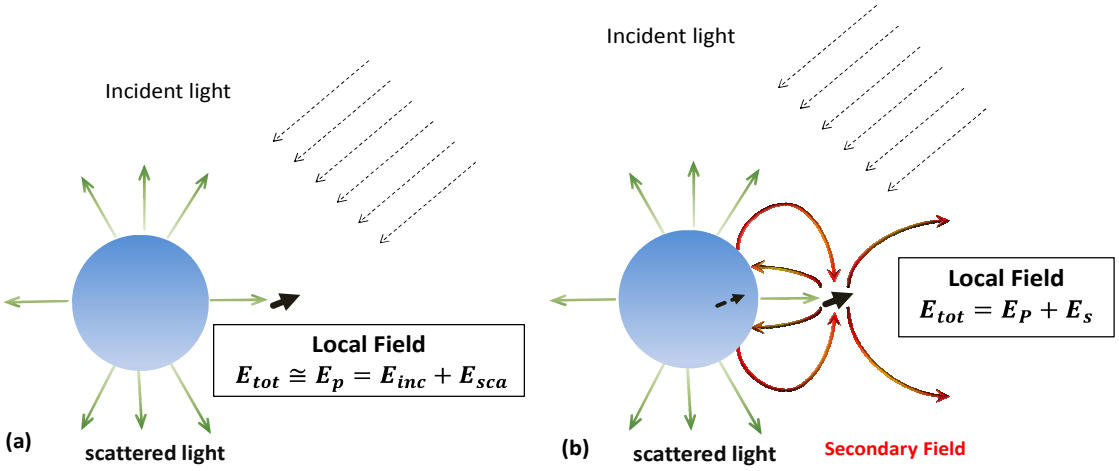

Fig. 5-2 (a) Simplified excitation enhancement model, (b) secondary field in consideration

The secondary field can be expressed using the dyadic Green function, connecting the electric field at position $\boldsymbol{r}$, due to the dipole $\boldsymbol{p}$ at position $\boldsymbol{r}_{\boldsymbol{m}}$ in the presence of nano sphere,

$$\boldsymbol{E}_s(\omega, \boldsymbol{r}) = \boldsymbol{S}(\boldsymbol{r}, \boldsymbol{r}_{\boldsymbol{m}}, \omega) \cdot \boldsymbol{p}(\omega) \tag{5-6}$$

where the specific Green function $\boldsymbol{S}(\boldsymbol{r}, \boldsymbol{r}_{\boldsymbol{m}}, \omega)$ can be found by the exact electromagnetic theory for emission [19, 20, 57]. We assume the dipole is linearly

polarized. Hence, the polarizability and the dipole moment can be re-written as $\boldsymbol{\alpha}(\omega) = \alpha(\omega)\mathbf{e}_d$ and $\boldsymbol{p}(\omega) = p(\omega)\mathbf{e}_d$. Combining Equation (5-6) and (5-7), the local total field in the polarization direction can be solved as,

$$\boldsymbol{e_d} \cdot \boldsymbol{E}_{tot}(\omega, \boldsymbol{r_m}) = \frac{\boldsymbol{e}_d \cdot \boldsymbol{E}_p(\omega, \boldsymbol{r_m})}{1 - \alpha(\omega)[\boldsymbol{e}_d \cdot \boldsymbol{S}(\boldsymbol{r_m}, \boldsymbol{r_m}, \omega) \cdot \boldsymbol{e}_d} \tag{5-7}$$

Yielding the induced dipole moment self-consistently as the combined result of the Mie field and the backscattering interaction:

$$p(\omega, \boldsymbol{r_m}) = \alpha(\omega) \frac{\boldsymbol{e}_d \cdot \boldsymbol{E}_p(\omega, \boldsymbol{r_m})}{1 - \alpha(\omega)[\boldsymbol{e}_d \cdot \boldsymbol{S}(\boldsymbol{r_m}, \boldsymbol{r_m}, \omega) \cdot \boldsymbol{e}_d} \tag{5-8}$$

Ignoring the backscattering interaction is tantamount to setting to zero the second term in the denominator. From Equation (3-7), we know the excitation enhancement is proportional to the square of the local electric field; which is the same as saying that it is proportional to the square of the dipole moment strength, therefore the enhancement in the presence of the scatterer relative to the absence of the scatterer is:

$$\begin{aligned} K_{ex}(\omega, \boldsymbol{r_m}) &= \frac{|\boldsymbol{e_d} \cdot \boldsymbol{E}_{tot}(\omega, \boldsymbol{r_m})|^2}{|\boldsymbol{e_d} \cdot \boldsymbol{E}_{inc}(\omega, \boldsymbol{r_m})|^2} = \frac{|p(\omega)|^2}{|p_0(\omega)|^2} \\ &= \left| \frac{\boldsymbol{e}_d \cdot \boldsymbol{E}_p(\omega, \boldsymbol{r_m})}{1 - \alpha(\omega)[\boldsymbol{e}_d \cdot \boldsymbol{S}(\boldsymbol{r_m}, \boldsymbol{r_m}, \omega) \cdot \boldsymbol{e}_p} \right|^2 \\ &= \frac{\left|\boldsymbol{e}_d \cdot \boldsymbol{E}_p(\boldsymbol{r_m}, \omega)\right|^2}{|\boldsymbol{e}_d \cdot \boldsymbol{E}_{inc}(\boldsymbol{r_m}, \omega)|^2} \frac{1}{|1 - \alpha(\omega)[\boldsymbol{e}_d \cdot \boldsymbol{S}(\boldsymbol{r_m} \boldsymbol{r_m}, \omega) \cdot \boldsymbol{e}_d]|^2} \\ &= I_{exc}(\omega, \boldsymbol{r_m}) \cdot D_{exc}(\omega, \boldsymbol{r_m}) \end{aligned} \tag{5-9}$$

The conventional simplified theory that ignores backscattering would expect only $I_{exc}(\omega, \boldsymbol{r_m})$ as enhancement factor. The difference between the simplified model and the

exact model we are using is the multiplicative factor $D_{exc}(\omega, \boldsymbol{r_m})$. This turns out to be always less than unity and so we call it the **derating factor**,

$$D_{exc}(\omega, \boldsymbol{r_m}) = \frac{1}{|1 - \alpha(\omega)[\boldsymbol{e}_d \cdot \boldsymbol{S}(\boldsymbol{r_m}, \boldsymbol{r_m}, \omega) \cdot \boldsymbol{e}_d]|^2} \tag{5-10}$$

The general expression for the exact excitation enhancement indicates that: (1) The excitation enhancement is still generally proportional to the sum of incident field and the scattering field from the sphere; but (2) this field is modified by molecular field. The polarizability and the Green function field (self-back-scattered field) determine the final magnitude of this derating factor. The polarizability is affected by the quantum yield of the molecule while the Green function of the interaction is strongly dependent on the orientation and position of the molecule relative to the scatterer (the sphere).

Following previous authors we call the Dyadic Green function $(\boldsymbol{r}', \boldsymbol{r}, \omega)$, the susceptibility [21, 58]; it describes the backscattering field from the sphere due to a the dipole of unit moment. For the highly symmetric case of the spherical scatterer the susceptibility ends up being independent of angle and only distance dependent,

$$\boldsymbol{e}_d \cdot \boldsymbol{S}(\boldsymbol{r_m}, \boldsymbol{r_m}, \omega) \cdot \boldsymbol{e}_d = S(d, d, \omega) \tag{5-11}$$

Consequently, the derating factor becomes a function of the polarizability $\alpha(\omega)$, orientation of the dipole $\boldsymbol{e}_p$, dielectric constant of the sphere and surrounding medium, and of course, the distance from the sphere to the dipole d. This angularly independent form simplifies the analysis of the spherical scatterer so that all relevant results can be obtained in closed form.

$$D_{exc}(\omega, d) = \frac{1}{|1 - \alpha(\omega) S(d, d, \omega)|^2} \tag{5-12}$$

In the following work, we explicitly solve the problem by decomposing the incident field, the Mie scattering field and the molecular self-scattering field into orthonormal spherical harmonics. Due to the dependence on the orientation of the molecule, we separate the interactions into two problems the tangential and the perpendicular cases relative to the surface of the sphere. The treatment is similar to the Gerstern-Nitzan theory and the exact Electrodynamical theory for the emission theory [17, 18].

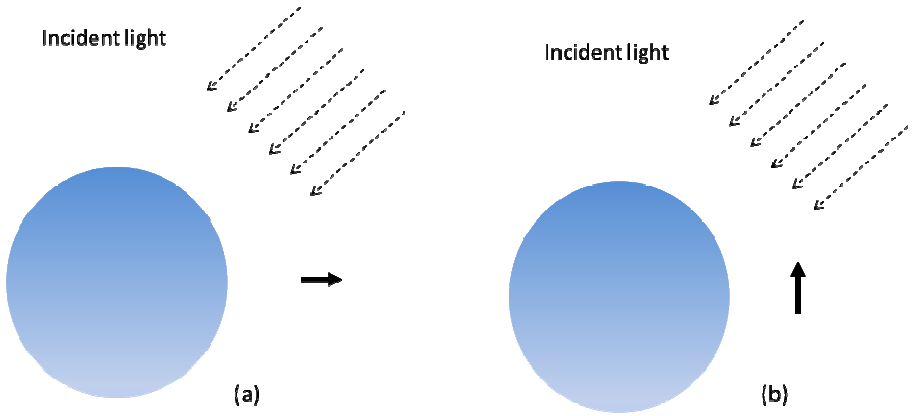

Fig. 5-3 (a) The perpendicular orientated dipole separated from (b) the tangental orientated dipole for both primary field and secondary field calculation

For the perpendicular dipolar molecule, the excitation enhancement factor has two parts: the local field enhancement from the incident field and scattering field in the perpendicular direction , and the derating factor from the molecule self-field that induces the secondary field effect. We will calculate each separately and combine them for the total excitation enhancement factor with frequency and distance dependence. The same procedure is followed for the tangential dipole.

5.4 The Primary field enhancement

Suppose the monochromatic incident wave is linearly polarized, the field $\boldsymbol{E}_{inc}(\boldsymbol{r_m}, \omega)$ could be written as $E_0 \boldsymbol{e_x} e^{ik_0 z}$. For the spherical system, we need to use (r, θ, ϕ) instead of (x, y, z) in the Cartesian coordinates. We utilize the orthonormal spherical harmonics in Jackson's notation [52].

$$\begin{aligned}\boldsymbol{E}_{inc}(\omega, \boldsymbol{r_m}) &= E_0 \boldsymbol{e_x} e^{ik_2 z} \\ &= E_0 \sum_{l=0}^{\infty} i^l \sqrt{\pi(2l+1)} [\frac{1}{k_2} \nabla \times j_l(k_2 d)(\boldsymbol{Y}_{ll1} - \boldsymbol{Y}_{ll-1}) \\ &+ j_l(k_2 d)(\boldsymbol{Y}_{ll1} + \boldsymbol{Y}_{ll-1})]\end{aligned} \tag{5-13}$$

where k_2 is the wave number of in the space $\omega\sqrt{\varepsilon_2 \mu_2}$. Here we define the orthonormal vector spherical harmonics as the vector angular function, with the property $\boldsymbol{r} \cdot \boldsymbol{L} \equiv 0$.

$$\boldsymbol{Y}_{llm} = \frac{1}{\sqrt{l(l+1)}} \boldsymbol{L} Y_{lm}(\theta, \phi) = \frac{1}{\sqrt{l(l+1)}} (\frac{\boldsymbol{r}' \times \boldsymbol{\nabla}}{i}) Y_{lm}(\theta, \phi) \tag{5-14}$$

The scattering field is calculated by Mie theory [52, 59],

$$\begin{aligned}\boldsymbol{E}_{sca}(\omega, \boldsymbol{r_m}) = E_0 \sum_{l=0}^{\infty} i^l \sqrt{\pi(2l+1)} [B_l \frac{1}{k_2} \nabla \times h_l^{(1)}(k_2 d)(\boldsymbol{Y}_{ll1} - \boldsymbol{Y}_{ll-1}) \\ + A_l h_l^{(1)}(k_2 d)(\boldsymbol{Y}_{ll1} + \boldsymbol{Y}_{ll-1})]\end{aligned} \tag{5-15}$$

Where the reflection coefficients for each modes is defined as,

$$A_l = \frac{\mu_2 j_l(k_2 a)[k_1 a j_l(k_1 a)]' - \mu_1 j_l(k_1 a)[k_2 a j_l(k_2 a)]'}{\mu_1 j_l(k_1 a)[k_2 a h_l^{(1)}(k_2 a)]' - \mu_2 j_l(k_2 a)[k_1 a h_l^{(1)}(k_1 a)]'} \tag{5-16}$$

$$B_l = \frac{\varepsilon_2 j_l(k_2 a)[k_1 a j_l(k_1 a)]' - \varepsilon_1 j_l(k_1 a)[k_2 a j_l(k_2 a)]'}{\varepsilon_1 j_l(k_1 a)[k_2 a h_l^{(1)}(k_2 a)]' - \varepsilon_2 j_l(k_2 a)[k_1 a h_l^{(1)}(k_1 a)]'} \tag{5-17}$$

a is the radius of the sphere, and k_1 is the wave number of in the sphere $\omega\sqrt{\varepsilon_1 \mu_1}$. The total primary field is,

$$\boldsymbol{E}_p(\omega, \boldsymbol{r_m}) = \boldsymbol{E}_{inc}(\omega, \boldsymbol{r_m}) + \boldsymbol{E}_{sca}(\omega, \boldsymbol{r_m}) \tag{5-18}$$

Finally, the general form for the primary field enhancement is

$$I_{exc}(\omega, \boldsymbol{r_m}) = \frac{\left|\boldsymbol{e}_d \cdot \boldsymbol{E}_p(\boldsymbol{r_m}, \omega)\right|^2}{|\boldsymbol{e}_d \cdot \boldsymbol{E}_{inc}(\boldsymbol{r_m}, \omega)|^2} \tag{5-19}$$

The enhancement is determined by the position of the molecule $\boldsymbol{r_m}$, orientation of the molecule $\boldsymbol{e}_d$, and sphere's electromagnetic property μ_1, ε_1 and radius a.

Generally, most experiments constrain the distance $d = r' - a$ between the sphere and the molecule by using DNA or RNA linking [1]. In most of these biological systems, the molecule and sphere have random position and orientation. Statistically, 1/3 of the molecule/sphere systems are considered as perpendicular, while the rest 2/3 have the molecule tangential relative to the surface of the sphere. The randomness occurs especially when the whole system operates in solution, or dispersed in the air. Hence, the enhancement factor due to the primary field can be calculated by averaging the electric field over the whole 4π steradian solid angle Ω.

The primary enhancement factors for perpendicular and tangential molecule cases are,

$$I_{exc\_p}(\omega,d)=\frac{\oiint\left|\boldsymbol{e}_r\cdot\boldsymbol{E}_p(\boldsymbol{r_m},\omega)\right|^2 d\Omega}{\oiint|\boldsymbol{e}_r\cdot\boldsymbol{E}_{inc}(\boldsymbol{r_m},\omega)|^2 d\Omega}$$
$$=\frac{3}{2}\sum_{l=1}^{\infty}(2l+1)(l+1)l\left|\frac{j_l(k_2d)+B_l h_l^{(1)}(k_2d)}{k_2d}\right|^2 \tag{5-20}$$

$$I_{exc\_t}(\omega,d)=\frac{\oiint\left|\boldsymbol{e}_\theta\cdot\boldsymbol{E}_p(\boldsymbol{r_m},\omega)\right|^2 d\Omega}{\oiint|\boldsymbol{e}_\theta\cdot\boldsymbol{E}_{inc}(\boldsymbol{r_m},\omega)|^2 d\Omega}=\frac{\oiint\left|\boldsymbol{e}_\phi\cdot\boldsymbol{E}_p(\boldsymbol{r_m},\omega)\right|^2 d\Omega}{\oiint\left|\boldsymbol{e}_\phi\cdot\boldsymbol{E}_{inc}(\boldsymbol{r_m},\omega)\right|^2 d\Omega}$$
$$=\frac{3}{4}\sum_{l=1}^{\infty}(2l+1)\left[\left|j_l(k_2d)+A_l h_l^{(1)}(k_2d)\right|^2\right. \tag{5-21}$$
$$\left.+\left|\frac{[k_2dh_l(k_2d)]'+B_l[k_2dh_l^{(1)}(k_2d)]'}{k_2d}\right|^2\right]$$

Here we used the decomposition of the spherical harmonics,

$$\frac{1}{k_2}\nabla\times f_l(k_2d)\boldsymbol{Y}_{llm}=\boldsymbol{e}_r\frac{i\sqrt{l(l+1)}}{k_2d}f_l(k_2d)Y_{lm}+\frac{1}{k_2d}[k_2df_l(k_2d)]' \tag{5-22}$$

We have thus obtained the enhancement factors in terms of spherical harmonics. Now we derive the derating factors.

5.5 The Derating factor

All we need is the unit dipole field scattered by the sphere from the exact Electrodynamical theory [19] evaluated at the position of the dipole. For the perpendicular dipole we get:

(5-23)

Similarly, for the tangential dipole we get the tangential back scattering field as

(5-24)

Plugging Equation (5-23) and (5-24) back into Equation (5-12), we will get the derating factor in closed form.

5.6 Numerical modeling for monochromatic illumination

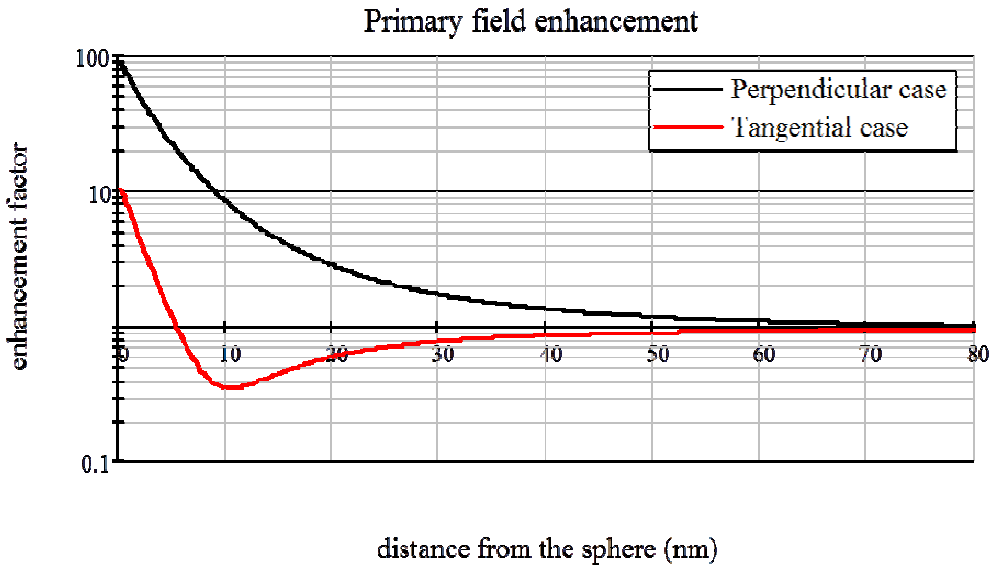

Fig. 5-4 Primary field enhancement of excitation without consideration of the secondary field effect

To illustrate the parameters that contribute to the enhancement we will first assume a fictitious molecule resonant at 430 nm in the vicinity of silver sphere [55] ($\varepsilon_1 = -5.08 + 1.12i, \mu_1 = 1$) as the dispersive plasmonic scatterer in water ($\varepsilon_2 = 1.77, \mu_2 = 1$). In Fig. 5-4, we show the results of only the primary field enhancement for the tangential and perpendicular dipole for the case of a 15 nm radius sphere.

The X axis is the distance from the molecule to the surface sphere ($d - a$). From the plot we can see that, the simplified model, which only uses the primary field enhancement factor, would predict high enhancement very close to the sphere (< 4nm) for both orientations of the molecule. Given the typical wide bandwidth of the Plasmon resonance of the sphere around 40nm, this result is weakly dependent on slight variations of the incident frequency.

To calculate the derating factor, we use the backscattering field $E(d, d, \omega)$ by a unit dipole (Equation (5-23) and (5-24)) and the classic polarizability of the molecule $\alpha(\omega)$ (Equation (5-3)). Classical radiative rates A_{21} are typically around $10^9 s^{-1}$, and we choose this as the standard value for the evaluation. Similar to the Definition of the quantum yield, we define Scattering yield $\mathrm{SY} = A_{21}/(A_{21} + k_{de})$. We know that the degeneration rate k_{de} is much larger than A_{21} generally. Thus, we set $k_{de} = 9A_{21}, 99A_{21}, 999A_{21}, 9990A_{21}$. Even so the molecule remains narrowband when compared with the sphere and we therefore can model cases with scattering yields of $10^{-1}, 10^{-2}, 10^{-3}, 10^{-4}$.

We plot the Derating factor for monochromatic illumination for the different scattering yields at exactly the absorption resonant frequency ω_{21}.

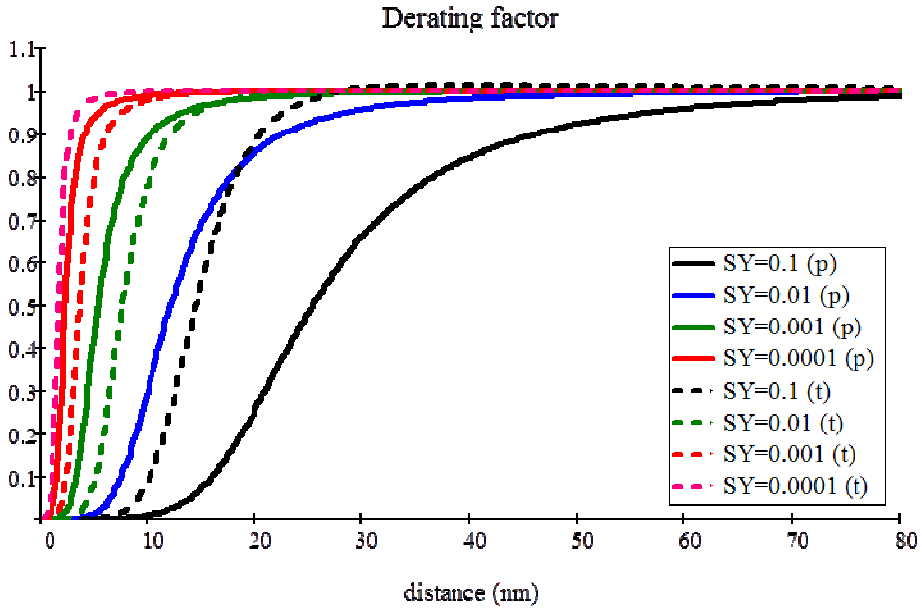

Fig. 5-5 Derating factor at resonance for difference orientations (T=tangential, P=perpendicular), and difference scattering yield

We combine the two factors together, we get the total excitation enhancement factors, and we compare them with the primary field enhancement in Fig. 5-5. The results demonstrate that if the illumination is monochromatic right on the absorption resonant frequency of the molecule, only when the distance is far away from the molecule, we get the same enhancement factors against the primary field enhancement. While the simplified theory that only use the primary field enhancement claims that close distance (0-10nm) has huge enhancement for molecule excitation, our theory with the consideration of the molecule backscattered field claim quenching for excitation. The reason could be that the plasmon sphere also has huge interaction with the week coherent emission, which couples the primary field and decreases the total local field on the molecule. The red curves in the Fig 6 demonstrate the case that he degeneration rate is

relatively large (, SY).The primary field could provide accurate excitation enhancement factor from far distance to about 5nm. However, near distances induce strong secondary field effects that the enhancement could turn into decrement. The maximum excitation enhancement factor was predicted as 27.7 at the optimum distance of 3.25nm away from the sphere. For the case of slow degeneration rate (, SY), there is no enhancement for excitation. If we have the moderate large degeneration rate (, SY), the optimum distance for excitation goes to 6.25nm away from the sphere, with the enhancement factor of 10.85.

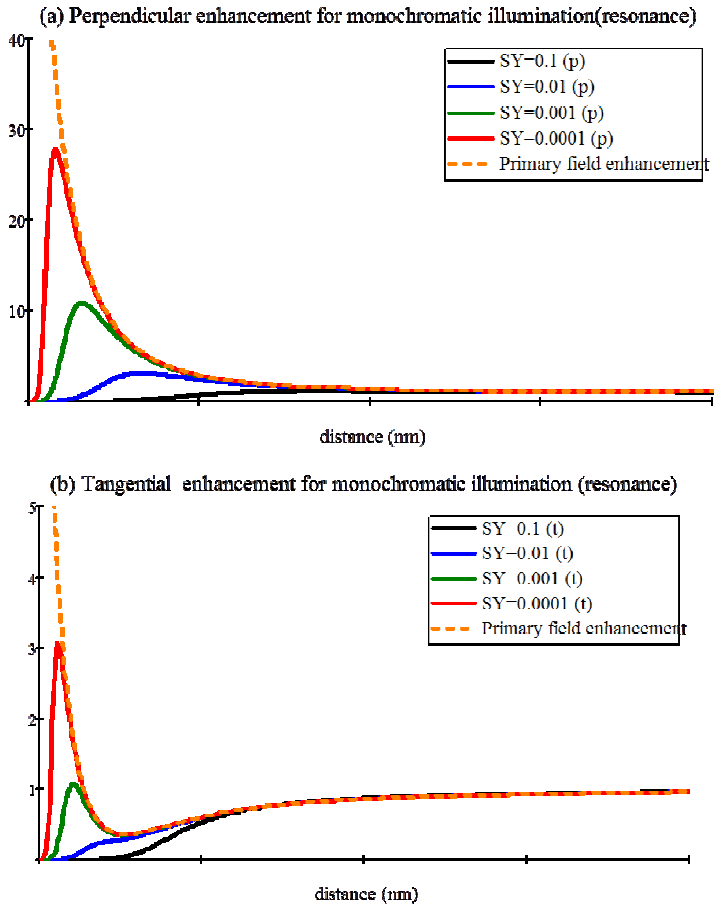

Fig. 5-6 The Excitation enhancement for monochromatic illumination (Dashed line: Simplified most. Solid lines: different scattering yield molecules)

5.7 Excitation/Absorption power spectrum and Frequency deviation

The previous numerical calculations demonstrated the significant changes on excitation enhancement at near distances. The assumption is that the absorption light is right on the resonant frequency of the molecule. This assumption is unrealistic, since the illumination light usually has a much broader bandwidth than the molecule. Also, the molecules would have difference on the resonant frequency due to the collisions from the medium. More realistic excitation enhancement has to consider the broadband absorbed energy. Of course, if the emission spectrum has the same bandwidth and the resonant frequency, then the monochromatic illumination results, which was shown in Fig 6 will be valid for broadband illumination. The absorption spectrum is calculated as

$$\begin{aligned}\rho(\omega,d) &= \frac{\oiint|\boldsymbol{\alpha}(\omega)\cdot\boldsymbol{E}_{tot}(\boldsymbol{r_m},\omega)|^2 d\Omega}{\oiint|\boldsymbol{\alpha}(\omega_{21})\cdot\boldsymbol{E}_{inc}|^2 d\Omega} \\ &\cong \frac{\oiint\left|\boldsymbol{e}_d\cdot\boldsymbol{E}_p(\boldsymbol{r_m},\omega_{21})\right|^2 d\Omega}{\oiint|\boldsymbol{e}_d\cdot\boldsymbol{E}_{inc}(\boldsymbol{r_m},\omega_{21})|^2 d\Omega}\frac{|\alpha(\omega)|^2}{|\alpha(\omega_{21})|^2}\,D_{exc}(\omega,d) \\ &= I_{exc}(\omega_{21},d)\,D_{exc}(\omega,d)\frac{|\alpha(\omega)|^2}{|\alpha(\omega_{21})|^2}\end{aligned} \tag{5-25}$$

This is normalized to $|\alpha(\omega_{21})\cdot\boldsymbol{E}_{inc}(\boldsymbol{r_m},\omega_{21})|^2$, the absorption power of the molecule at the resonance frequency in the absence of the sphere. Using a moderate scattering yield SY $= 10^{-3}$ we plot the normalized absorption spectrum $\rho(\omega,d)$ against the wavelength λ, at various distances from the sphere in Fig. 5-7**Error! Reference source not found.**. We see that for a distance of the order of the radius of the sphere (15nm), the spectrum still maintains the same bandwidth and resonance frequency as the isolated molecule. But as the molecule gets closer to the sphere, 430nm is no longer the resonance

frequency for excitation. The whole spectrum is red-shifted and the mutual interactions also alter the bandwidth. The perpendicular molecule is in general more vulnerable to the sphere's EM interaction than the tangential.

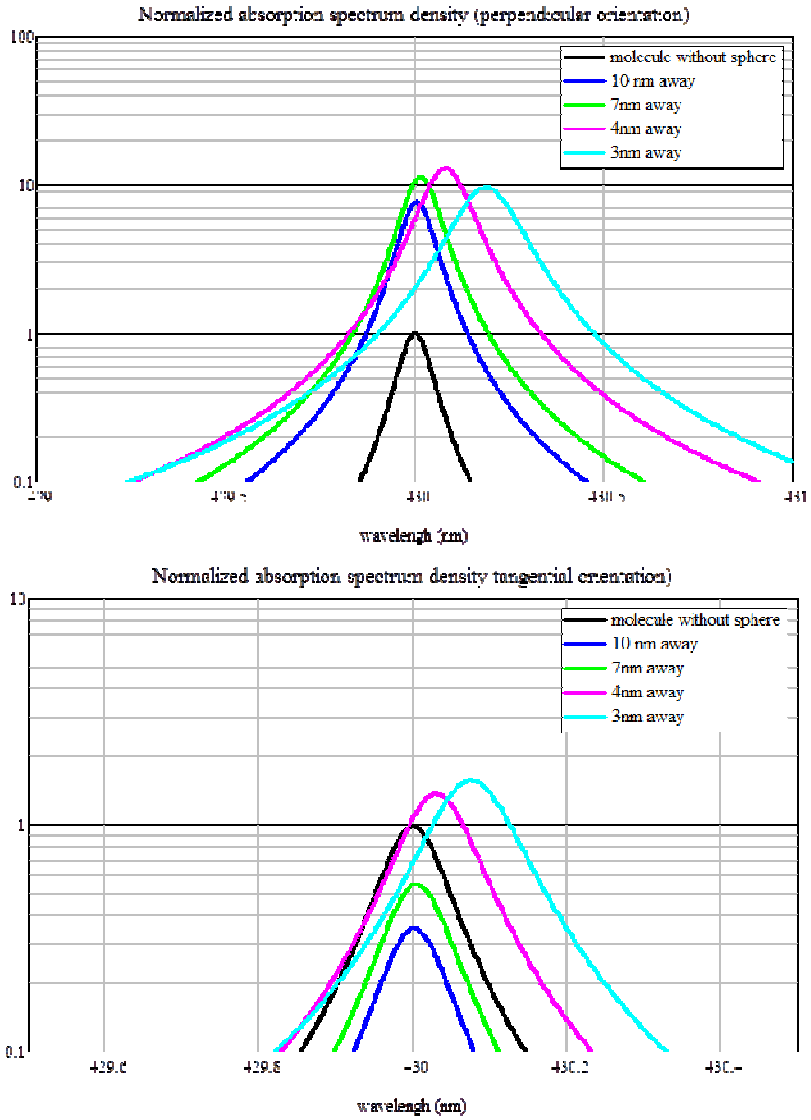

Fig. 5-7 Normalized absorption spectrum (top: perpendicular orientation; bottom: tangential orientation)

5.8 Realistic excitation enhancement under broadband illumination

Now we can calculate the real excitation enhancement under broadband illumination by integrating over the whole spectrum, taking the bandwidth and resonance frequency shifts into account. Similar to the spectrum density definition, we define this realistic excitation enhancement factor as follows:

(5-26)

We utilized the property that the molecule absorption bands are always narrower than the total primary field enhancement calculated from the Mie theory, which is nearly frequency independent within the narrow absorption region.

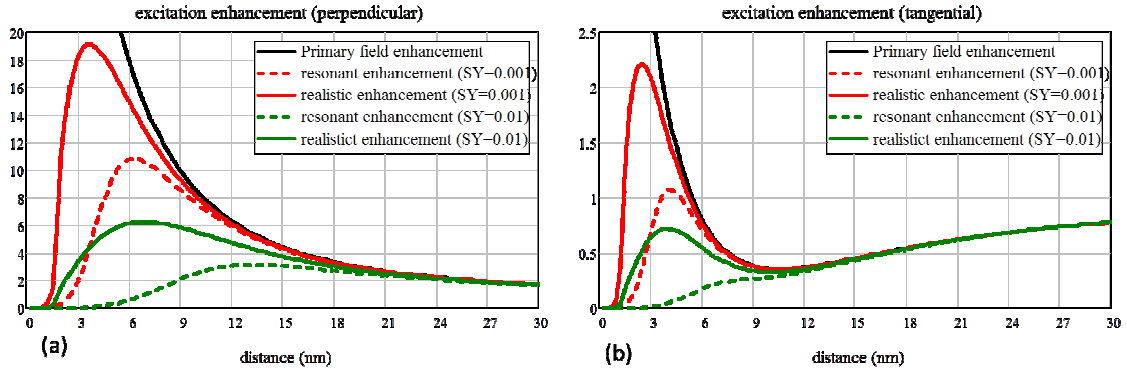

Fig. 5-8 realistic excitation enhancement, with the comparison with the primary field enhancement

We use as two examples to compare the enhancement predictions. In this case all three enhancements are approximately the same beyond 15nm from the surface (one sphere radius). Similar to previous resonance enhancement

calculation, the perpendicularly oriented molecule has the stronger secondary field effects for broadband excitation/absorption.

For the fast degeneration case ($SY = 0.001$),when the molecule/sphere distance is less than 6 nm, the most realistic model for either tangential or perpendicular disagrees with both the simplified primary field model and the realistic model where only the resonant frequency is used. Using only the resonant frequency case leads to an overly pessimistic result. However, although integration over the spectrum has recovered some of the enhancement, the true enhancement can still be significantly lower than we would be led to believe if we used only the primary field enhancement. The real excitation enhancement factor for the perpendicularly oriented molecule could be as high as 19, while the resonance model underestimates this by about half. For the tangential molecule, the resonant model predicts nearly no enhancement, while the actual enhancement could be more than 2. For the slow degeneration case ($SY = 0.01$), the backscattering secondary field effects become stronger. We still observe the difference between the resonant models and realistic model. Beside the actual strength of any enhancement, the two models can also differ significantly on the expected optimum distance for maximum enhancement.

5.9 Influence on the total fluorescence enhancement

We have seen that quenching can begin during the absorption phase of the interaction. To completely model a typical fluorescence experiment we need to add the interaction during emission. In the conventional model that assumes only primary field

enhancement quenching only appears during emission as the molecule excites so called "dark modes' in the sphere and dissipates energy. In the realistic model this extra quenching compounds the total quenching. We assume a small Stokes shift and choose the emission wavelength of the molecule to be around 440nm. Then the silver sphere has the permittivity of . We consider two different molecule cases: (1) low quantum yield ; (2) high quantum yield

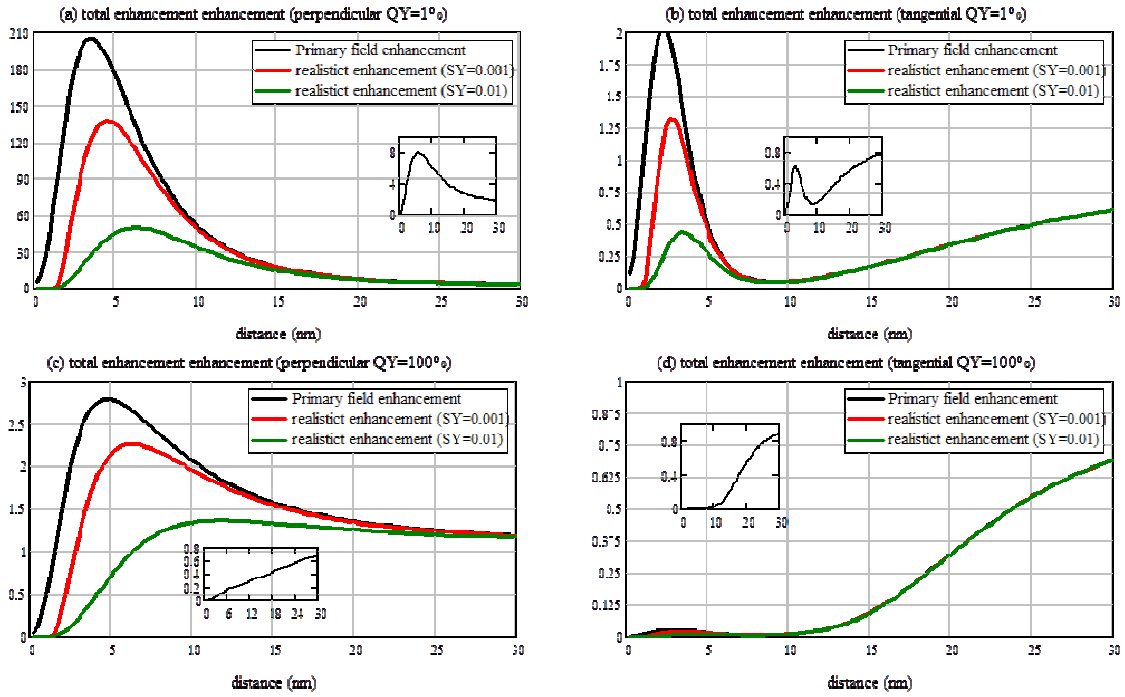

Fig. 5-9 Total Fluorescence enhancement for different scattering yield (red: SY=0.001. green: SY=0.01) compared to the simplified theory using only the primary field (black).

First, consider the low quantum yield case. In Fig. 5-9(a), we compare the total fluorescence enhancement in the realistic model to the model that only uses the primary excitation for the case of the perpendicular molecule. For both, the emission process provides 8 times enhancement. So, the total enhancement predicted by the simplified

primary field model gives 205 as the highest enhancement factor. However, the realistic model tells us that the highest enhancement factor is also related to the molecular polarizability, which is related to the degeneration rate. If the molecule has low scattering yield $SY = 0.001$, the fluorescence enhancement for the perpendicular enhancement factor could be as high as 137 at the optimum distance of 4.5nm; if the molecule has high scattering yield $SY = 0.01$, the fluorescence enhancement for the perpendicular molecule drops to 50 at the optimum distance 6.5nm.

According to the result plotted in Fig. 5-9(b), the total fluorescence enhancement for the tangential molecule could still be 2 times, if there were no re-radiation secondary field. With the consideration of the secondary field effect, the fluorescence would not be as large as the simplified theory predicted. Specifically, for the case of $SY = 0.01$, the molecule fluorescence is actually quenched by the sphere.

Now we consider the high quantum yield (100%) molecule. The emission efficiency could never go higher than 100%. Therefore, the emission process can only quench the total fluorescence. For the perpendicularly oriented molecule, the simplified theory using the primary field enhancement predicts a 2.7 times enhancement, while realistic molecules would only fluoresce 1.4-2.2 times higher. The optimum distance can be very different depending on the scattering yield of the molecule. For the tangential-oriented molecule, both the emission process and the excitation process will undermine the enhancement. Within 10 nm distance, both models claim that the tangential molecule will be quenched dramatically.

5.10 Conclusion

In this chapter, we have analyzed the excitation enhancement experienced by a molecule in the vicinity of a single Noble metal nano-sphere. It has been shown that the molecular spontaneous emission during the absorption process can interfere with the incident wave and the scattered wave from the sphere. Including the spontaneous emission by introducing the polarizability of the molecule for excitation local field calculation leads to an additional field we call the "secondary field". For the monochromatic illumination, the resulting excitation enhancement is different from the primary field enhancement that would be obtained using only the Mie theory. The molecule-sphere interaction causes a red shift in the molecule's absorption frequency, a broadening of the absorption spectrum, and always leads to a derating factor that reduces the total field at the molecule. Integrating over the absorption spectrum leads to the most realistic excitation enhancement calculation. Combining the final realistic model for the excitation with the exact Electrodynamical model for the emission, we calculate the total fluorescence enhancement. This result is strongly dependent on both the molecule's quantum yield and the molecule's scattering yield (dominated by the degeneration rate from the excited state to the lowest excited level from which emission occurs).

Because high quantum yield molecules are always quenched during emission, the total fluorescence enhancement obtained using only the primary excitation field only differs slightly from the more accurate calculation that includes the derating due to the secondary field. However, for low quantum yield molecules we find that weakly scattering molecules (fast degeneration rates) can reap a large enhancement from the

nanoparticle while strongly scattering molecules (slow degeneration rates) can receive additional quenching during the absorption part of the interaction. Similarly, including the derating factor in the calculation can significantly alter the predicted optimal distance from the surface to observe enhancement. The results are presented for the two extreme orientations of the molecule relative to the sphere surface: perpendicular and tangential. Enhancement, when it occurs, is always stronger for the perpendicular case. But if an experiment randomly averages the orientation of the molecule relative to the sphere, the observed experimental results will be weighted 2/3 tangential versus 1/3 perpendicular, resulting in measured enhancements that are typically 1/3 of the maximum theoretically possible.

Chapter 6

GENERAL METHOD FOR THE TOTAL FLUORESNCENCE ENHANCEMENT ESTIMATION

In this chapter, we generalize the calculation of the total fluorescence enhancement by arbitrary-shape antenna. The Methods simply separate the total enhancement into three parts: primary field enhancement, derating factor, and the emission quantum yield efficiency enhancement. Following the electrodynamical methods for the monomer spherical antenna, we understand the excitation enhancement is not a trivial problem. The derating factor is as important as the primary field enhancement, due to the strong interaction between the incident wave, the molecule and the enhancing antenna.

6.1 Separations for the surface enhanced fluorescence

In the quantum mechanical description on the back-scattered field [14], the *dressed* dipole moment was introduced to describe the relations of the molecular dipolar re-radiation from the spontaneous emission A_{21} and incident wave $\boldsymbol{E_{inc}}$. Obviously, the methods forced the effects on calculating the additional radiation and additional losses in the terms of decay rates. Here, we propose a simple and self-consistent method to calculate the polarization of the molecule. We found the frequency shifts and boarding effects inherently in our modeling for the single sphere [22]. In our way of calculation, we don't calculate the dipole moment by the "dressed" polarizability. Instead, we used the "naked" polarizability $\vec{\vec{\boldsymbol{\alpha}}}_0(\omega)$ (free molecule) of multiples the local field

$\boldsymbol{E}_{tot}(\boldsymbol{r_m}, \omega_{21})$ instead of the incident field $\boldsymbol{E_{inc}}(\boldsymbol{r_m}, \omega_{21})$. The interaction between the molecule and the sphere is implemented in the total field $\boldsymbol{E}_{tot}$.

$$\boldsymbol{p}(\boldsymbol{r_m}, \omega) = \vec{\overleftrightarrow{\boldsymbol{\alpha}}}_0(\omega) \cdot \boldsymbol{E}_{tot}(\boldsymbol{r_m}, \omega) \tag{6-1}$$

The linearly polarized assumption could simplified into Equation (6-2),

$$\boldsymbol{p}(\omega) = [\boldsymbol{\alpha_0}(\omega) \cdot \boldsymbol{E}_{tot}(\boldsymbol{r_m}, \omega)]\boldsymbol{e}_d = [\boldsymbol{\alpha}(\omega) \cdot (\boldsymbol{E}_d(\boldsymbol{r_m}, \omega) + \boldsymbol{E}_s(\boldsymbol{r_m}, \omega))]\boldsymbol{e}_d \tag{6-2}$$

We define the primary field $\boldsymbol{E}_p(\boldsymbol{r_m}, \omega)$ as the sum of the incident fiel d $\boldsymbol{E_{inc}}(\boldsymbol{r_m}, \omega)$ and the scattered field $\boldsymbol{E_{sca}}(\boldsymbol{r_m}, \omega)$. Here, the perturbation from the molecule is included in the form of the total field,

$$\begin{aligned} \boldsymbol{E}_{tot}(\boldsymbol{r_m}, \omega) &= \boldsymbol{E_{inc}}(\boldsymbol{r_m}, \omega) + \boldsymbol{E_{sca}}(\boldsymbol{r_m}, \omega) + \boldsymbol{E_s}(\boldsymbol{r_m}, \omega) \\ &= \boldsymbol{E_p}(\boldsymbol{r_m}, \omega) + \boldsymbol{E_s}(\boldsymbol{r_m}, \omega) \end{aligned} \tag{6-3}$$

Another reason for using Equation (6-2) and (6-3), is that the total field calculation might involves complicate and/or large scaled structure, where the analytical forms for the *"dressed"* dipole moment no longer exists in the analytical from.

The total fluorescence enhancement maintains the original form of the multiplication by excitation enhancement and emission enhancement. However, we realize that the total field might be different than the simple form. We define the intrinsic polarizability by its radiative rate A_{21} and its degeneration rate K_{de}. γ_{21} is the total decay rate from Level II into level I, that is approximately $A_{21} + K_{de}$, if we assumed that the internal loss rate in the excitation is much smaller than the degeneration rate .

$$\boldsymbol{\alpha_0}(\omega) = \frac{{d_{21}}^2}{\hbar}\left(\frac{1}{\omega_{21} - \omega - i\gamma_{21}} + \frac{1}{\omega_{21} + \omega + i\gamma_{21}}\right)\mathbf{e}_d \tag{6-4}$$

$${d_{21}}^2 = \frac{6\pi\varepsilon_0\hbar c^3}{\omega_{21}^3} A_{21} \tag{6-5}$$

Generally, we assume the incident wave illuminated the molecule at resonance. Similar to the quantum yield definition, we define the scattering yield as $SY = A_{21}/(K_{de} + A_{21})$, to represent the ratio between radiative rate and the total decay rate for absorption.

The final excitation enhancement K_{ex} can be separated into two parts as we have done for the spherical antenna,

$$K_{ex}(\omega, \boldsymbol{r_m}) = \frac{\left|\boldsymbol{e}_d \cdot \boldsymbol{E}_p(\boldsymbol{r_m}, \omega)\right|^2}{|\boldsymbol{e}_d \cdot \boldsymbol{E}_{inc}(\boldsymbol{r_m}, \omega)|^2} \frac{1}{|1 - \alpha(\omega)[\boldsymbol{e}_d \cdot \boldsymbol{S}(\boldsymbol{r_m}\boldsymbol{r_m}, \omega) \cdot \boldsymbol{e}_d]|^2} \\ = I_{exc}(\omega, \boldsymbol{r_m}) \cdot D_{exc}(\omega, \boldsymbol{r_m}) \tag{6-6}$$

the field enhancement by the primary field $I_{exc}(\omega, \boldsymbol{r_m})$, and the secondary field derating factor $D_{exc}(\omega, \boldsymbol{r_m})$ The secondary field effects is calculated from two factors: the unit dipole susceptibility [21, 20]to the environment —the unit electric dipole backscattered field back onto the molecule, and the polarizability $\alpha_0(\omega)$. At the resonant frequency, the polarizability becomes $\alpha_0(\omega_{21}) = i\frac{3\pi\varepsilon_0 c^3}{\omega_{21}^3} SY$. The dipole strength at the absorption resonant frequency is *proportional* to the scattering yield.

For the metal enhanced fluorescence, we could generally separate the program into three parts: Primary field enhancement I_{exc}, the secondary field derating factor D_{exc}, and the emission efficiency adjustment K_{em} (Quantum yield enhancement). In the Table 6-1, we summarized the electromagnetic methods to calculate all these enhancement factors and necessary parameters.

	scheme	Parameters	Enhancement factors
Primary field enhancement	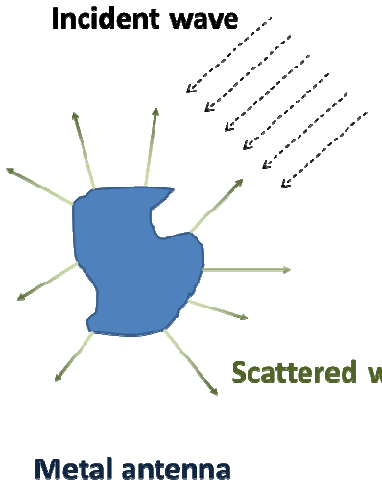	at excitation frequency	$\frac{\lvert E_{loc}(\omega_{exc})\rvert^2}{\lvert E_0(\omega_{exc})\rvert^2}$
Derating factor	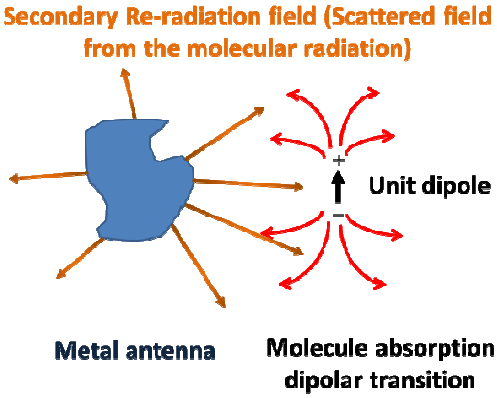	Scattered field back on the molecule	$\frac{\lvert E_{loc}(\omega_{em})\rvert^2}{\lvert E_0(\omega_{em})\rvert^2}$
Emission efficiency enhancement	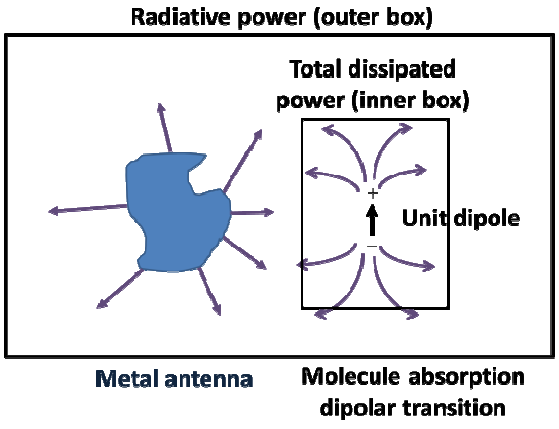	$\frac{P_{rad}}{P_{abs}}$ $\frac{P_{rad}}{P_{abs}}$ Operating at emission frequency	Emission QY enhancement $\frac{QY_{loc}}{QY_0}$ $\frac{\eta_{loc}}{\eta_0}$

Table 6-1 Fluorescence enhancement separation and scheme for electrodynamical enhancement factors' calculation

Instead of simulating the frequency-dependent derating factors by implementing the dipolar molecule into the numerical programs, we could perform an additional simulation for the back-scattered field. This near field effect simulation provides us the flexibility to adjustment the polarizability for different scattering yields or different illumination frequencies.

The emission efficiency adjustment could be simulated by placing an unit dipole radiating with the vicinity of the nano-antenna. The ratio between the raditation power and the total dissipated power, by definition, provide the quantum yield for the system. The benefit for this method is that, we could alter the intrinsic quantum yield to observe the emission enhancement differences for difference molecules.

6.2 FDTD simulation and numerical results

In this session, we would apply the separated way for calculation on the excitation enhancement to some specific nano-antennas. We utilize the finite differential time domain method (FDTD) as our numerical tool. Using silver as an example, we model metal as a single Drude material at the optical frequency. We will compare the scattering cross section of single sphere calculated from the Mie theory to the results from the simulations. The primary field enhancement I_{exc} and the derating factor D_{exc} will be calculated for the resonant illumination. The numerical results will be compared with the analytical results for the near field validation.

We assumed that the excitation wavelength of the molecule is 430nm (generally the porphyrin absorption wavelength). We knew that in the RF range, most metals can be considered as good conductors. However, in the optical wavelength, the effective permittivities of metals carry low conduction terms and behave dispersive. Multi-Drude/Lorentz models are generally used for broadband data matching. The relative permeabilities of metals are generally unity ($\mu_r \equiv 1$) at the optical frequency. Silver is one of the most common noble metals that are used for biological experiments. A single Drude material was used to match the relative permittivity ε_1 of silver is modeled as one single Drude material as in Equation (6-7).

$$\varepsilon_1(\omega) = \varepsilon_\infty[1 - \frac{\omega_p^2}{\omega(\omega + i\Gamma_D)}] \tag{6-7}$$

Where we set the parameter as the following: the high frequency permittivity $\varepsilon_\infty = 5.08$, the Plasmon frequency $\omega_p = 6.283 \times 10^{15} s^{-1}$ and the damping term $\Gamma_D = 5.327 \times 10^{14} s^{-1}$. We plot the permittivity of silver single drude model V.S

the Using the refractive index from the article [55] , we calculate the permittivity and consider the mean free path effects for small sphere(d=20nm) [42]. We match the permittivity on 430nm to make sure that the single Drude modeling is accurate for the calculation for the absorption. In Figure 1, we demonstrated the drude material matching with the measured data. According to Figure 6-1, the single Drude model has good matches in both the real parts and the imaginary parts of Ag's permittivity calculated from the refractive index from the article [55]. Even though the discrepancy is observable off the resonance, the results would be valid since a single molecule absorption bandwidth is extremely narrow (<0.2nm).

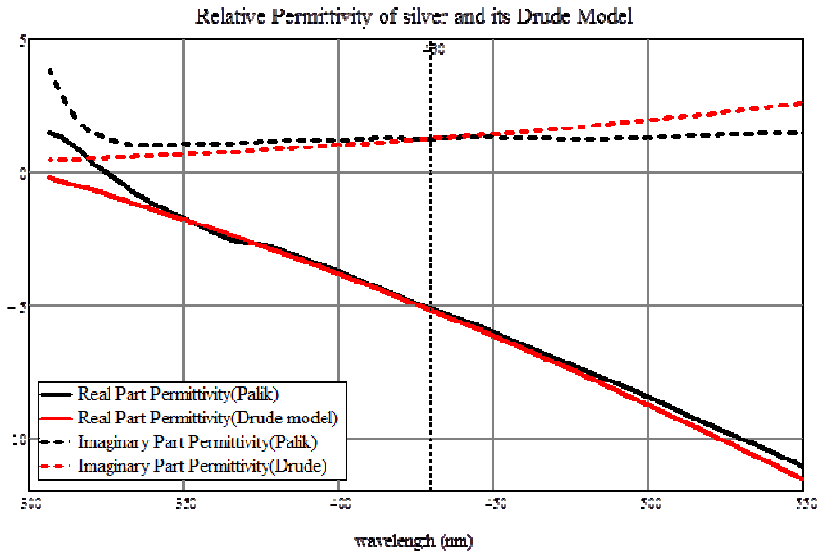

Fig. 6-1 Single Drude Modeling for the permittivity of 20nm silver sphere around 430 nm

The Drude material is implemented using the auxiliary differential equation method [60]. The spatial discretization is 1nm, and we used two stacked re-radiating boundaries for the termination [61].

First, we perform the plane wave illumination on the 20nm Ag sphere, the far field are used to calculating the scattering cross section. In Fig 6-2., we could see a very

good match against the Mie theory: The resonant wavelength is at 395nm and the bandwidth is the same. At the illumination wavelength 430nm for the resonance fluorescence, FDTD has identical far-field cross-section to the Mie theory. The validation demonstrates that our way to implement the dispersive material is correct.

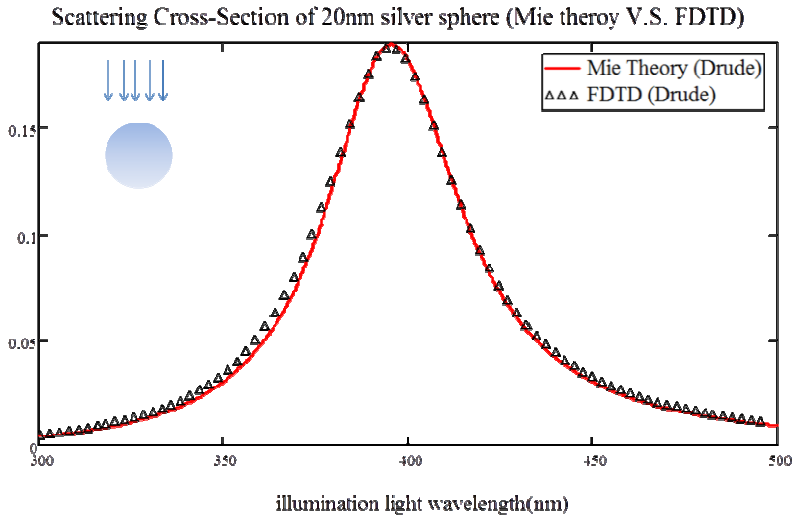

Fig. 6-2 FDTD Validation: Scattering Cross Section of the 20nm sphere with comparison with Mie theory

Spherical structure:

The single sphere was widely used for fluorescence enhancement experiments due to the symmetrical structures and standardized manufacture process. Since we have our analytical models for the sphere, we could compare the results with spheres.

Primary field enhancement parameters are calculated by illuminating the plane wave into the nano-antenna, and calculate the local field as we shown Table 6-1.In Fig. 6-3, the FDTD provide accurate primary field enhancement vs. the Mie field theory. The difference in near distance is because the coarseness of the structure (ds=1nm) created the roughness on the surface that detour the local field for near distance. The deviation only

happens in 2nm distance away from the sphere, which is only twice of the coarseness. Hence, in all the following FDTD simulations, we will not place the molecule too close to the sphere — 2nm would be the minimum distance we observe.

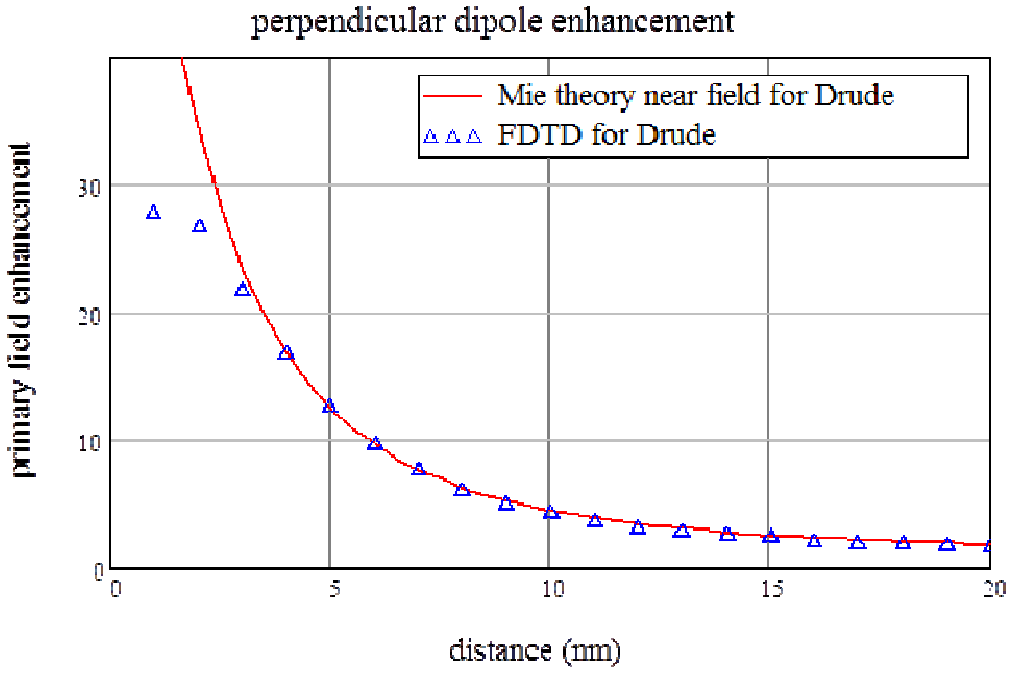

Fig. 6-3 the primary field enhancement by single sphere (monomer)

Now, we extract the backscattering field by the molecule. The dipole moment is assigned as unity, and we record the local field on the dipole, and then subtract the field from dipole-in-solution system (without sphere). The back-scatter field strength by the unit dipole is also compared with the exact electrodynamical model. In Fig. 6-4 , we plot the backscatter field strength and phase by the unit dipole source. With the comparison against electrodynamical theory, the simulation results from FDTD has good consistency with our theory. Deviations in the near distance may be induced by the coarseness of the sphere.

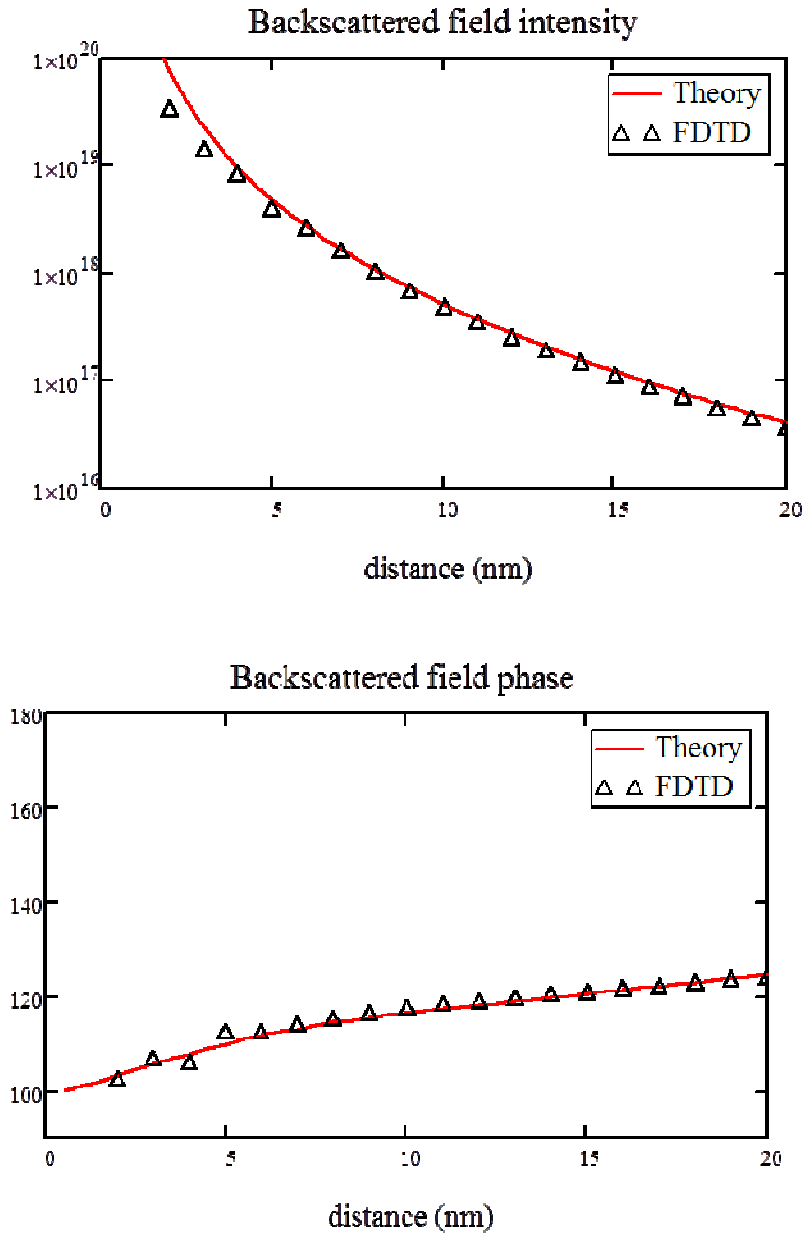

Fig. 6-4 Backscattered field from the sphere on the discrete unit dipole (amplitude and phase)

The porphyrin molecule in the solution is about to have its intrinsic scattering yield as 1/1000. By implementing the scattering yield into the derating calculation, we

plot the total excitation enhancement from FDTD, and exact EM solution from Chapter 5. The enhancement factors are also compared with the simplified theory that only used the Mie field. According to Fig. 6-5, numerical simulations demonstrate good reliability on the near field and the far field: the FDTD could provide fairly accurate optimum distance (in this car 5-6nm) and the maximum enhancement (around 6 times).

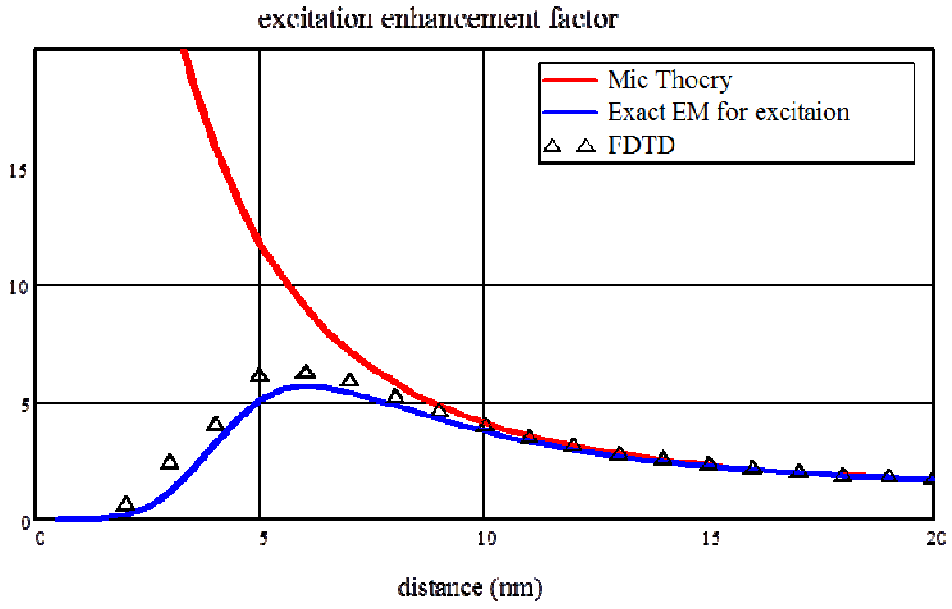

Fig. 6-5 the total excitation enhancement calculation by FDTD with the comparison against the exact electrodynamical theory

Dimer structure:

The monomer sphere enhancement simulation is validated. For better enhancement for excitation, Dimer is proposed. We still align the molecular polarization in the direction of the incident electrical field. The dimer is also aligned in the same direction. Here we want to observe the near field enhancement of the dimer, since people claim high intensive field in the middle of the two spheres. We separate the distance

between two spheres as 4nm, 6nm, 8nm and 10nm. Assuming the molecule is in the middle of the structure, the distance from the molecule to the sphere would be 2nm, 3nm, 4nm and 5nm.

	Monomer sphere		Dimer sphere	
Molecule to sphere distance(nm)	Primary field enhancement	Total excitation enhancement	Primary field enhancement	Total excitation enhancement
2	26.8	0.69	1100	4.96
3	21.8	2.48	348	5.92
4	16.8	4.12	175	10.33
5	9.7	6.20	99.86	15.28

Table 6-2 Resonant excitation enhancement from dimers

In Table 6-2, we summarized our FDTD simulation comparisons of excitation enhancement. Even though the primary field enhancement could provide as much as 1000 times enhancement between two spheres, however, the backscattered field has the secondary field effects that kills the total excitation enhancement. We could only get about 15 times enhancement if the illumination is just on the molecule resonance. Even though it is better than the sphere, total enhancement could never be as high as thousands times as people predicted.

6.3 Conclusion

In this Chapter, we discuss the method for generalizing the electrodynamical solution for complicate nano-antennas. The finite time difference time method is used to

investigate the problem from the numerical calculations. The excitation enhancement by the monomer sphere is calculated. The numerical results for both the primary field enhancement factors and the backscattering derating factors are consistent with the exact electromagnetic theory we developed in Chapter 5. For better enhancement, we also investigated the dimer structure which was promised for high enhancement. However, the strong secondary fields derate the total excitation enhancement dramatically. The numerical results indicate that dimers would be helpful for fluorescence enhancement. But we could never expect significantly increment by orders. FDTD could also be used for other complicate structures for the investigation on excitation enhancement and fluorescence enhancement since the near field has very few deviation from the theory.

Chapter 7

SUMMARY

In this dissertation, we applied the classical electromagnetics to the surface enhanced fluorescence. We divided the fluorescence problem into excitation and emission. We compared our model on the excitation with the conventional simplified model. With the combination of the exact electromagnetic theory and the classical decription molecular excitation, we observed the strong secondary field due to the molecular self-re-radiation. The secondary field alters the local field around the molecule which contributes to the excitation enhancement. The derating factor is introduced for the secondary effect description. Based on the comparison with the conventional simplified theory, our theory could explain both experimental results with completely different setup. The comparison indicates the existence of the backscattering effects, which incur the derating effects on excitation enhancement. Analytical solutions for the spherical antenna are derived. The perpendicular orientation and the tangential orientation are separated for simplification. The total fluorescence enhancement is also calculated for low QY molecule and high QY molecule. The excitation enhancement has strong influence for the low QY molecule, which we anticipate high enhancement. In near distance, the excitation enhancement is strongly quenched by the secondary field, and the total enhancement for low QY could never be as high as the Mie theory predicted. Once we have the complete electromagnetic theory for the excitation and emission in the sphere, we also apply the whole theory for any arbitrary shape optical antenna by numerical methods. FDTD demonstrated excellent consistency with the analytical

theories for the spheres. Both near field and far field could be obtained accurately. The simulations for Dimer's enhancement indicate the possibility of higher enhancement. However, the derating rating was more destructive for such intensive field concentration structures.

REFERENCES

[1] E. Dulkeith, A. C. Morteani, T. Niedereichholz, T. A. Klar, J. Feldmann , S. A. Levi, F. C. J. M. van Veggel, D. N. Reinhoudt , M. Möller and D. I. Gittins , "Fluorescence Quenching of Dye Molecules near Gold Nanoparticles: Radiative and Nonradiative Effects," *Phys. Rev. Lett.*, vol. 89, p. 203002, 2002.

[2] E. Dulkeith, M. Ringler, T. A. Klar, J. Feldmann, A. Muñoz Javier and W. J. Parak, "Gold Nanoparticles Quench Fluorescence by Phase Induced Radiative Rate Suppression," *Nano Lett.*, vol. 5, p. 585–589, 2005.

[3] L. Bene, G. Szentesi, L. Mátyus, R. Gáspár and S. Damjanovich, "Nanoparticle energy transfer on the cell surface," *Journal of Molecular Recognition*, vol. 18, no. 3, pp. 236-253, 2005.

[4] G. Schneider, G. Decher, N. Nerambourg , R. Praho , M. H. V. Werts and M. Blanchard-Desce, "Distance-Dependent Fluorescence Quenching on Gold Nanoparticles Ensheathed with Layer-by-Layer Assembled Polyelectrolytes," *Nano Lett.*, vol. 6, no. 3, p. 530–536, 2006.

[5] J. Zhang , I. Gryczynski, Z. Gryczynski and J. R. Lakowicz, "Dye-Labeled Silver Nanoshell−Bright Particle," *J. Phys. Chem. B*, vol. 110, no. 18, p. 8986–8991, 2006.

[6] P. Anger, P. Bharadwaj and L. Novotny, "Enhancement and quenching of single-molecule fluorescence," *Phys. Rev. Lett.*, vol. 96, p. 113002, 2006.

[7] P. Bharadwaj and L. Novotny, "Spectral dependence of single molecule fluorescence enhancement," *Optics Express*, vol. 15, no. 21, p. 14266, 2007.

[8] J. R. Lakowicz, B. Shen, Z. Gryczynski, S. D'Auria and I. Gryczynski, "Intrinsic Fluorescence from DNA can be Enhanced by Metallic Particles," *Biochemical and Biophysical Research Communications*, vol. 286, p. 875–879, 2001.

[9] Y. Fu, J. Zhang and J. R. Lakowicz, "Plasmon-Enhanced Fluorescence from Single Fluorophores End-Linked to Gold Nanorods," *J. Am. Chem. Soc.*, vol. 132 , no. 16, p. 5540–5541, 2010.

[10] E. Fort and S. Grésillon, "Surface enhanced fluorescence," *J. Phys. D: Appl. Phys.*, vol. 41, p. 013001, 2008.

[11] G. Colas des Francs, A. Bouhelier, E. Finot, J. C. Weeber, A. Dereux, C. Girard and E. Dujardin, "Fluorescence relaxation in the near–field of a mesoscopic metallic particle: distance dependence and role of plasmon modes," *Optics Express*, vol. 16, no. 22, pp. 17654-17666, 2008.

[12] G. Sun, J. B. Khurgin and R. A. Soref, "Plasmonic light-emission enhancement with isolated metal nanoparticles and their coupled arrays," *J. Opt. Soc. Am. B*, vol. 25, no. 10, pp. 1748-1755, 2008.

[13] P. Das and H. Metiu, "Enhancement of molecular fluorescence and photochemistry by small metal particles," *J. Phys. Chem.*, vol. 89, p. 4680–4687, 1985.

[14] P. C. Das and A. Puri , "Energy flow and fluorescence near a small metal particle," *Phys. Rev. B*, vol. 65, no. 15, p. 155416 , 2002.

[15] E. Purcell, "Spontaneous emission probabilities at radio frequencies," *Phys. Rev.*,

vol. 69, p. 681, 1946.

[16] H. Chew, P. J. McNulty and M. Kerker , "Model for Raman and fluorescent scattering by molecules embedded in small particles," *Phys. Rev. A*, vol. 13, no. 1, p. 396–404, 1976.

[17] J. Gersten and A. Nitzan, "Spectroscopic properties of molecules interacting with small dielectric particles," *J. Chem. Phys.*, vol. 75, p. 1139, 1981.

[18] R. Ruppin, "Decay of an excited molecule near a small metal sphere," *J. Chem. Phys.*, vol. 76, p. 1681, 1982.

[19] H. Chew, "Transition rates of atoms near spherical surfaces," *J. Chem. Phys.*, vol. 87, p. 1355, 1987.

[20] Y. S. Kim, P. Leung and T. F. George, "Classical decay rates for molecules in the presence of a spherical surface: A complete treatment," *Surface Science,* vol. 195, pp. 1-14, 1988.

[21] R. Carminati, J. J. Greffet, C. Henkel and J. Vigoureux, "Radiative and non-radiative decay of a single molecule close to a metallic nanoparticle," *Optics Communications,* vol. 261, no. 2, p. 368–375, 2006.

[22] Z. Zhang and R. E. Diaz, "Fluorescence excitation enhancement by single Plasmon sphere — the importance of secondary field effect," *TO BE PUBLISHED,* 2013.

[23] C. A. Balanis, Antenna theory: analysis and design, Wiley-Interscience, 2012.

[24] J. Griffin, A. K. Singh, D. Senapati , P. Rhodes, K. Mitchell, B. Robinson, E. Yu and P. C. Ray, "Size- and Distance-Dependent Nanoparticle Surface-Energy Transfer (NSET) Method for Selective Sensing of Hepatitis C Virus RNA," *Chemistry - A European Journal,* vol. 15, no. 2, p. 342–351, 2009.

[25] J. H. Lee, J. H. Park, J. S. Kima, D. Y. Leeb and K. Cho, "High efficiency polymer solar cells with wet deposited plasmonic gold nanodots," *Organic Electronics*, vol. 10, no. 3, p. 416–420, 2009.

[26] C. Hägglund, M. Zäch and B. Kasemo, "Enhanced charge carrier generation in dye sensitized solar cells by nanoparticle plasmons," *Appl. Phys. Lett.*, vol. 92, p. 013113 , 2008.

[27] C. S. Yun, A. Javier, T. Jennings, M. Fisher, S. Hira, S. Peterson, B. Hopkins, N. O. Reich and G. F. Strouse, "Nanometal Surface Energy Transfer in Optical Rulers, Breaking the FRET Barrier," *J. Am. Chem. Soc*, vol. 127, no. 9, p. 3115–3119, 2005.

[28] J. Zhang, Y. Fu, M. H. Chowdhury and J. R. Lakowicz, "Single-Molecule Studies on Fluorescently Labeled Silver Particles: Effects of Particle Size," *J. Phys. Chem. C*, vol. 112, no. 1, p. 18–26, 2008.

[29] L. K. Ausman and G. C. Schatz, "On the importance of incorporating dipole reradiation in the modeling of surface enhanced Raman scattering from spheres," *J. Chem. Phys.* , vol. 131, no. 8, p. 084708, 2009.

[30] G. Sun and J. B. Khurgin, "Origin of giant difference between fluorescence, resonance, and nonresonance Raman scattering enhancement by surface plasmons," *Phys. Rev. A* , vol. 85, p. 063410, 2012.

[31] I. A. Larkin, M. I. Stockman, M. Achermann and V. I. Klimov, "Dipolar emitters at

nanoscale proximity of metal surfaces: Giant enhancement of relaxation in microscopic theory," *Phys. Rev. B,* vol. 69, no. 12, p. 121403, 2004.

[32] P. T. Leung, "Decay of molecules at spherical surfaces: Nonlocal effects," *Phys. Rev. B,* vol. 69, no. 12, p. 121403, 2004.

[33] S. A. Schelkunoff and H. T. Friis, Antennas: theory and practice, Wiley, 1952.

[34] D. Lim, Fluorescence Enhancing Photonic Devices, ASU, 2006.

[35] D. Lim and R. E. Diaz, "Classical emulation of molecular fluorescence and the modification of its quantum efficiency by nearby material structures," in *Joint International Conference on Electromagnetics in Advanced Applications and EuropeanElectromagnetic Structures Conference*, Torino, 2005.

[36] O. Kulakovich, N. Strekal, A. Yaroshevich, S. Maskevich, S. Gaponenko, I. Nabiev, U. Woggon and M. Artemyev , "Enhanced Luminescence of CdSe Quantum Dots on Gold Colloids," *Nano Letters,* vol. 2, no. 12, p. 1449–1452, 2002.

[37] C. Louis, S. Roux, G. Ledoux, L. Lemelle and . P. Gill, "Gold Nano-Antennas for Increasing Luminescence," *Advanced Materials,* vol. 16, no. 23-24, p. 2163–2166, 2004.

[38] S. Kühn, U. Håkanson, L. Rogobete and V. Sandoghdar, "Enhancement of Single-Molecule Fluorescence Using a Gold Nanoparticle as an Optical Nanoantenna," *Phys. Rev. Lett.,* vol. 97, p. 017402, 2006.

[39] M. H. Chowdhury, K. Aslan, S. N. Malyn and J. R. Lakowicz, "Metal-enhanced chemiluminescence: Radiating plasmons generated from chemically induced electronic excited states," *Applied Physics Letters,* vol. 88, no. 17, p. 173104, 2006.

[40] A. M. Brouwer, "Standards for photoluminescence quantum," *Pure Appl. Chem.,* vol. 83, no. 12, p. 2213–2228, 2011.

[41] K. C. Toh, A. E. Stojković, H. M. van Stokkum, K. Moffat and J. T. M. Kennis, "Fluorescence quantum yield and photochemistry of bacteriophytochrome constructs," *Chem. Phys.,* vol. 13, pp. 11985-11997, 2011.

[42] W. Zhang, S. H. Brongersmaa, O. Richard, B. Brijs, R. Palmans, L. Froyen and K. Maex, "Influence of the electron mean free path on the resistivity of thin metal films," *Microelectronic Engineering,* vol. 76, p. 146–152, 2004.

[43] Z. B. Wang, B. S. Luk'yanchuk, M. H. Hong, Y. Lin and T. C. Chong, "Energy flow around a small particle investigated by classical Mie theory," *Phys. Rev. B.,* vol. 70, p. 035418, 2004.

[44] Z. Zhang, D. Lim and R. E. Diaz, "Image theory for plasmon-modified luminescence near nanospheres," in *Proc. SPIE 8595, Colloidal Nanocrystals for Biomedical Applications VIII*, San Francisco, 2013.

[45] V. V. Klimov, M. Ducloy and V. S. Letokhov, "Radiative frequency shift and linewidth of an atom dipole in the vicinity of a dielectric microsphere," *Journal of Modern Optics,* vol. 43, no. 11, pp. 2251-2267, 1996.

[46] F. Tam, G. P. Goodrich, B. R. Johnson and N. J. Halas, "Plasmonic Enhancement of Molecular Fluorescence," *Nano Lett.,* vol. 7, no. 2, p. 496–501, 2007.

[47] K. H. Drexhage, "IV Interaction of Light with Monomolecular Dye Layers,"

Progress in Optics, vol. 12, p. 193–232, 1974.

[48] J.-K. Hwang, H.-Y. Ryu and Y.-H. Lee, "Spontaneous emission rate of an electric dipole in a general microcavity," *Phys. Rev. B,* vol. 60, no. 7, p. 4688–4695, 1999.

[49] Y. Xu, R. K. Lee and A. Yariv, "Finite-difference time-domain analysis of spontaneous emission in a microdisk cavity," *Phys. Rev. A,* vol. 61, no. 3, p. 033808, 2000.

[50] R. Loudon and S. M. Barnett , "Theory of the linear polarizability of a two-level atom," *Journal of Physics B: Atomic, Molecular and Optical Physics,* vol. 39, p. S555, 2006.

[51] P. W. Milonni , R. Loudon , P. R. Berman and S. M. Barnett , "Linear polarizabilities of two- and three-level atoms," *Phys. Rev. A* , vol. 77, p. 043835 , 2008.

[52] J. D. Jackson, Classical Electrodynamics, Wiley-VCH, 1998 .

[53] I. V. Lindell, "Electrostatic image theory for the dielectric sphere," *Radio Science,* vol. 27, no. 1, pp. 1-8, 1992.

[54] W. T. Norris, "Charge images in a dielectric sphere," *IEE Proceedings-Science, Measurement and Technology,* vol. 142, no. 2, pp. 142-150, 1995.

[55] E. D. Palik, Handbook of Optical Constants of Solids, Boston: Academic Press, 1991.

[56] Y. Zhang, R. Zhang, Q. Wang, Z. Zhang, H. Zhu, J. Liu, F. Song, S. Lin and E. Yue Bun Pun, "Fluorescence enhancement of quantum emitters with different energy systems near a single spherical metal nanoparticle," *Optics Express,* vol. 18, no. 5, pp. 4316-4328, 2010.

[57] H. Mertens, A. F. Koenderink and A. Polman, "Plasmon-enhanced luminescence near noble-metal nanospheres: Comparison of exact theory and an improved Gersten and Nitzan model," *Phys. Rev. B* , vol. 76, p. 115123 , 2007.

[58] J. . M. Wylie and J. E. Sipe , "Quantum electrodynamics near an interface," *Phys. Rev. A,* vol. 30, no. 3, p. 1185–1193, 1984.

[59] C. . F. Bohren and D. R. Huffman, Absorption and scattering of light by small particles, New York: Wiley-Interscience, 1983.

[60] A. Taflove and S. C. Hagness, Computational electrodynamics., Boston: Artech house, 2000.

[61] R. E. Diaz and I. Scherbatko, "A simple stackable re-radiating boundary condition (rRBC) for FDTD," *IEEE:Antennas and Propagation Magazine,* vol. 46, no. 1, pp. 124-130, 2004.

[62] J. R. Lakowicz and Y. Fu, "Modification of single molecule fluorescence near metallic nanostructures," *Laser & Photonics Reviews,* vol. 3, p. 221–232, 2009.

[63] O. L. Muskens , . V. Giannini , . J. A. Sánchez-Gil and J. Gómez Rivas, "Strong Enhancement of the Radiative Decay Rate of Emitters by Single Plasmonic Nanoantennas," *Nano Lett.,* vol. 7, p. 2871–2875, 2007.

[64] T. Soller, M. Ringler, M. Wunderlich, T. A. Klar and J. Feldmann, "Radiative and Nonradiative Rates of Phosphors Attached to Gold Nanoparticles," *Nano Lett.,* vol.

7, p. 1941–1946, 2007.

[65] W. Zhang, S. H. Brongersma, B. Brijs, . R. Palmans, L. Froyen and . K. Maex, "Influence of the electron mean free path on the resistivity of thin metal films," *Materials for Advanced Metallization,* vol. 76, p. 146–152, 2004.

[66] R. C. Hilborn, "Einstein coefficients, cross sections, f values, dipole moments, and all that," *American Journal of Physics,* vol. 50, no. 11, p. 982, 1982 .